Stratigraphic architecture of the world's oldest shale gas play: The 1400-1200 Ma Velkerri and Kyalla formations in the Beetaloo Sub-Basin.

Vincent Crombez[1#], Marcus Kunzmann[2*], Mohinudeen Faiz[3], Claudio Delle Piane[1], Stuart Munday[4], Anne Forbes[4]

[1] *Deep Earth Imaging – Future Science Platform, Kensington, 6151, Australia*
[2] *Mineral Resources, CSIRO, 26 Dick Perry Avenue, Kensington, 6151, Australia*
[3] *Energy, CSIRO, 1 Technology Court, Pullenvale, 4069, Australia*
[4] *Chemostrat Australia, 1131 Hay Street, West Perth, 6005, Australia*
[#] *corresponding author (vincent.crombez@csiro.au), * current address: Fortescue Metals Group Ltd, East Perth, 6004, Australia*

The Mesoproterozoic Velkerri and Kyalla formations in the Beetaloo Sub-basin in northern Australia contain the world's oldest shale plays. In unconventional exploration, the main challenge is the identification of sweet spots from which hydrocarbons can be produced economically. In fine-grained siliciclastic intervals, the distribution of these sweet spots is mainly controlled by the evolution of the sedimentary system and its effects on organic matter distribution. The aim of the present work is therefore to reconstruct the stratigraphic architecture of the Velkerri-Kyalla interval and to integrate its stratigraphic evolution with chemostratigraphic and chronostratigraphic frameworks. Based on core descriptions and well correlations, we reconstructed the facies distribution within the Velkerri-Kyalla interval along two regional well sections. This allowed for the recognition of stratigraphic stacking patterns and to identify multiple depositional sequences. Three stratigraphic orders are observed within the Velkerri-Kyalla formations. The studied interval is interpreted to be deposited during one second-order depositional sequence, containing four nested third-order depositional sequences. These, in turn, are composed of thirteen nested fourth-order transgressive-regressive sequences. By integrating the sequence stratigraphic architecture with available geochronological constraints, we postulate a chronostratigraphic framework for these Mesoproterozoic strata. The Velkerri Formation was likely deposited between 1400 Ma and 1280 Ma, and the overlying Kyalla Formation between 1250 Ma and 1190 Ma. Furthermore, by coupling the sequence stratigraphy, chemostratigraphy and existing provenance studies, and chronostratigraphy, we were able to construct regional paleogeographic maps to illustrate the evolution of the basin in the broader context of the Mesoproterozoic of northern Australia.

Acknowledgments

1. Introduction

Sweet spots in unconventional plays are formed by the co-occurrence of three elements: (1) hydrocarbon enrichment (2) suitable geomechanical properties leading to fracture conductivity, and (3) good reservoir drive (OTTMANN AND BOHACS, 2014). This means economic plays consist of hydrocarbon-bearing intervals with suitable reservoir conditions to recover high volumes of oil and/or gas after hydraulic stimulation. Two elements directly relate to the distribution of sedimentary heterogeneities in the play: hydrocarbon enrichment and geomechanical properties that are both controlled by the sedimentary facies including mineral and organic contents. Understanding the distribution of sedimentary heterogeneities is therefore of paramount importance for predicting the distribution of sweet spots in self-sourced reservoirs. In frontier exploration, the scale of the sedimentary heterogeneities that control the distribution and quality of these reservoirs is often sub-seismic (<40 m). Therefore, seismic reflection data are only suitable to constrain the top and base of a play and exploration largely relies on the interpretation of well data to understand its stratigraphic evolution and to predict areas with higher prospectivity potential.

The increasing interest in shale plays and the development of model-independent sequence stratigraphy (CATUNEANU, 2006; CATUNEANU ET AL., 2009, 2010, 2019A) have resulted in numerous basin-scale studies of fine-grained siliciclastic rocks (PASSEY ET AL., 2010; KIETZMANN ET AL., 2014; KOHL ET AL., 2014; BORCOVSKY ET AL., 2017; BYUN ET AL., 2018; CROMBEZ ET AL., 2019; KNAPP ET AL., 2019). These studies mainly focussed on understanding the distribution of sedimentary facies and their stacking patterns (e.g., VAN BUCHEM ET AL., 2005), and on defining or refining a stratigraphic framework (e.g., SMITH AND BUSTIN, 2000; ANGULO AND BUATOIS, 2012; BORCOVSKY ET AL., 2017). Important for exploration, understanding the stratigraphic architecture of a play allows for a test of its potential seismic expression (e.g. ZELLER ET AL., 2015), and is also a prerequisite for sweet spot prediction using process-based models (e.g. CROMBEZ ET AL., 2017).

Unconventional shale reservoir exploration in Australia currently focuses on the Mesoproterozoic Beetaloo Sub-basin located in northern Australia (Figure 1). Map-based estimates of the resources suggest 899 Bbbl (P50) of oil in place (OIP) for the Kyalla Formation, and 85 Bbbl (P50) of OIP and 208 TCF (P50) of gas in place in the Amungee Member of the Velkerri Formation (REVIE, 2017B). Although this resource potential has stimulated significant exploration activity (HOFFMAN, 2015; CLOSE ET AL., 2017; SHERIDAN ET AL., 2018; BRUCE AND GARRAD, 2021), the high-resolution, basin-scale stratigraphic architecture of this Mesoproterozoic interval has not yet been published.

Here, we reconstruct the stratigraphic architecture of the Velkerri, Moroak and Kyalla formations in the Beetaloo Sub-basin. Using publicly available wireline log and geochemical data from wells arranged along N-S and E-W cross-sections we (1) reconstruct the spatial and stratigraphic facies distribution, (2) identify stacking patterns, and (3) reconstruct a sequence stratigraphic framework. This process allows us to assess the controls on the sedimentary architecture, to integrate the cyclicity in chrono- and chemostratigraphic frameworks, and to discuss the basin-scale paleogeographic evolution of the Beetaloo Sub-basin.
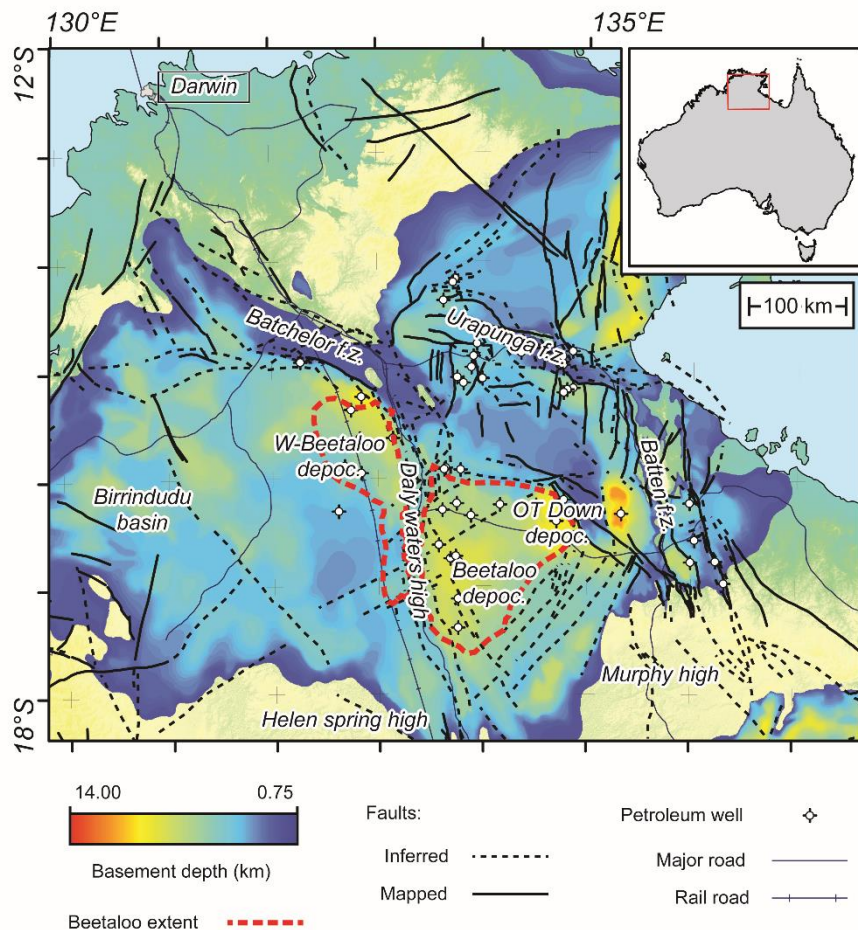
Figure 1: Location of the study area. This basement depth map highlights the extent of the greater McArthur area and the location of the Beetaloo Sub-basin. Note the occurrences of the deepest depocenters in structurally complex areas and over the Beetaloo sub-basins (Data from FROGTECH, 2018, Beetaloo Sub-Basin extend from WILLIAMS, 2019).

2. Geological background

2.1. The greater McArthur Basin and the Beetaloo Sub-Basin

The greater McArthur Basin is an inclusive definition of the Paleoproterozoic to Mesoproterozoic sedimentary basins located in the Northern Territory of Australia (RAWLINGS, 1999; AHMAD ET AL., 2013; CLOSE, 2014). The thickest parts of the basin are thought to exceed 12 km (Figure 1, FROGTECH, 2018), and are located in structurally complex areas or the area defined as the Beetaloo Sub-basin (Beetaloo). The Beetaloo was first defined as a sub-basin based on a gravity and magnetic anomaly (JACKSON ET AL., 1987; PLUMB AND WELLMAN, 1987). Today, this concealed sub-basin is interpreted to extend over more than 60 000 km². The limits of the Beetaloo Sub-basin have been recently updated and formalized by the Northern Territory Geological Survey and have been constrained using lithostratigraphic data from wells tied to stratigraphic interpretations of the available 2D seismic surveys (WILLIAMS, 2019). Accordingly, the sub-basin boundary is currently defined using the top of the Kyalla Formation, constrained by a cut-off depth of 400 m below surface (WILLIAMS, 2019). It is important to note that the current geophysical definition does not correspond to the extent of the sediments of interest for hydrocarbon exploration and hydrocarbon plays have been identified beyond the extents of the geophysically defined boundary (BRUCE AND GARRAD, 2021).

The Beetaloo lies on the North Australian Craton (NAC) and is bound to the north by the Batchelor and Urapunga fault zones, to the east by the Batten Fault Zone and the Murphy high, to the south by the Helen Springs high, and the west by the Birrindudu Basin. It comprises three distinct depocenters including the eastern Beetaloo depocenter separated from the western Beetaloo depocenter by the Daly Waters high and the OT Downs depocenter (Figure 1). Although the petroleum wells and regional seismic data highlight relatively flat-lying Proterozoic strata (Figure 2A), the greater McArthur Basin fill records the formation and break-up of different supercontinents (e.g. MEERT AND SANTOSH, 2017; MULDER ET AL., 2015; MYERS ET AL., 1996; PISAREVSKY ET AL., 2014). Its stratigraphy is traditionally subdivided into four non-genetic packages, the youngest package is the Wilton package and comprises the Roper Group (RAWLINGS, 1999). Geochronology studies based on detrital zircons, Re-Os analyses, and intrusions dating, suggest Mesoproterozoic ages for the Roper Group (JACKSON ET AL., 2000; KENDALL ET AL., 2009; YANG ET AL., 2018), which contains the Velkerri and Kyalla formations (Figure 2B). This interval mainly comprises siliciclastic sedimentary rocks (POWELL ET AL., 1987; DONNELLY AND CRICK, 1988; JACKSON ET AL., 1988; ABBOTT AND SWEET, 2000; MUNSON, 2016), that have been intruded by Mesoproterozoic dolerite dykes and sills (TUCKER AND BOYD, 1987; ABBOTT ET AL., 2001).
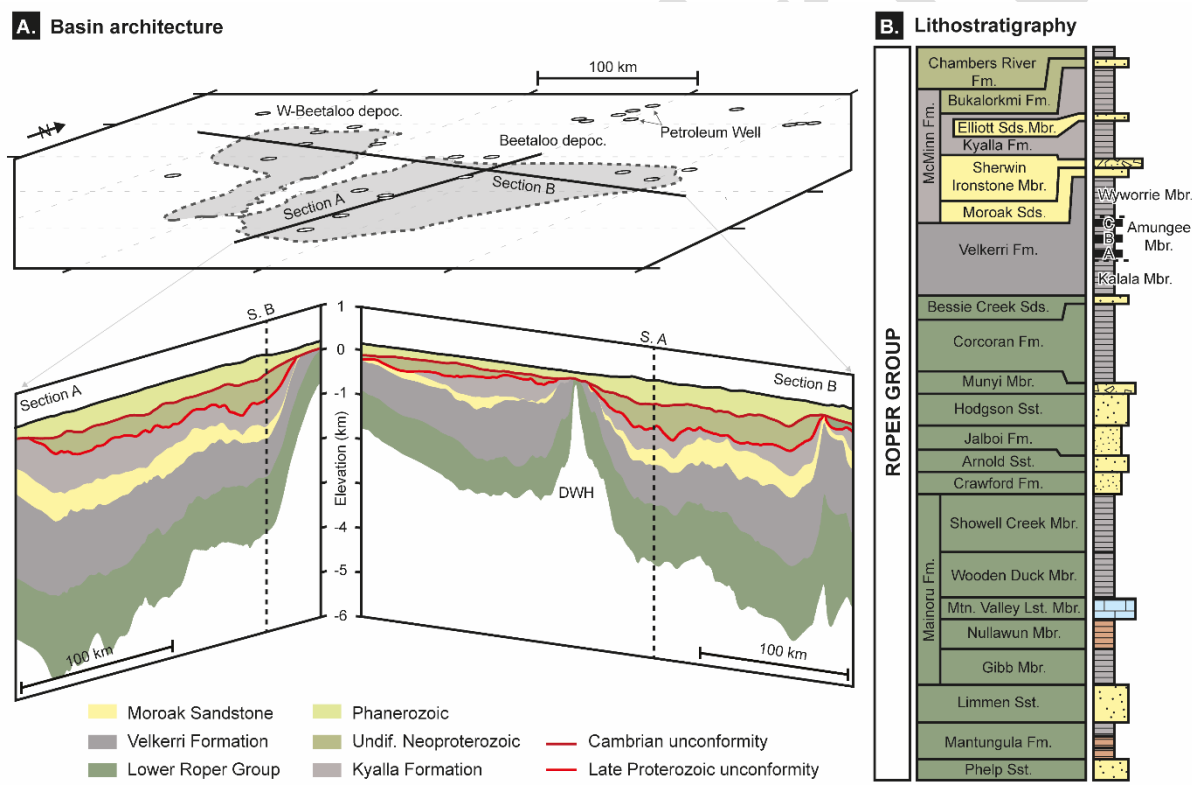
Figure 2: A. Two-dimensional cross-sections from the sub-surface of the Beetaloo Sub-basin. Note the Daly Waters High (DWH) dividing the sub-basin into two depocenters. B. Simplified lithostratigraphy of the Roper Group (modified from RAWLINGS, 1999). This study focuses on the Velkerri to Kyalla interval.

Paleogeographic reconstructions suggest the NAC occupied a position around 30°N during the deposition of the Roper Group (PISAREVSKY ET AL., 2014; MEERT AND SANTOSH, 2017). At this time, the NAC was located to the east of western Laurentia. In these geodynamical reconstructions, the deposition of the Roper Group is linked to the break-up of the Nuna supercontinent and the initiation of a rift system between Laurentia and the NAC (MULDER ET AL., 2015). The major unconformity at the base of the Roper Group is attributed to the Isan Orogeny (DE VRIES ET AL., 2008; BLAIKIE AND KUNZMANN, 2020), and includes inversion of pre-existing structures (LINDSAY, 2001). Although the deposition of the

Roper Group started in an active geodynamical setting, most recent studies suggest an intra-cratonic setting influenced by flexural tectonics was responsible for the deposition of the interval comprising the Velkerri to Kyalla formations (LANIGAN ET AL., 1994; ABBOTT AND SWEET, 2000).

2.2. The Velkerri-Kyalla interval

The Velkerri, Moroak and Kyalla formations occur in the upper part of the Roper Group (Figure 2B). The Velkerri Formation is divided into three members, from oldest to youngest: the Kalala, Amungee and Wyworrie members (MUNSON AND REVIE, 2018). The precise duration and age of the Velkerri Formation are still debated. Re-Os dating suggests that the Velkerri Formation was deposited from 1417±29 Ma to 1361±21 Ma (KENDALL ET AL., 2009). Based on detrital zircon geochronology, YANG ET AL. (2018) proposed maximum depositional ages of 1308±41 Ma and 1313±47 Ma for the Velkerri Formation. More recent work by YANG ET AL. (2020) suggests deposition of the Kyalla Formation prior to 1092±16 Ma.

The lithological characteristics of the Velkerri, Moroak and Kyalla formations were extensively studied by POWELL ET AL., (1987), MUNSON (2016) AND MUNSON AND REVIE (2018). The Velkerri Formation is mainly composed of interlaminated and interbedded siltstone and claystone, with minor fine-grained sandstone and rare dolomitised limestone. The conformably to unconformably overlying Moroak Sandstone likely represents the proximal part of the sedimentary system (POWELL ET AL., 1987; WARREN ET AL., 1998; ABBOTT AND SWEET, 2000). It consists predominantly of fine- to medium-grained sandstone, interlayered with minor coarse-grained standstone, conglomereate and siltstone (MUNSON, 2016). The conformably overlying Kyalla Formation is mainly composed of siltstone, silty claystone and rare occurrences of claystone. However, a thick sandstone interval, referred to as the Elliott sandstone member, can be distinguished between the lower and upper parts (MUNSON, 2016). It is generally accepted that the Velkerri, Moroak, and Kyalla formations were deposited on a continental shelf (ABBOTT AND SWEET, 2000; MUNSON, 2016) with depositional environments ranging from shallow marine deltaic to offshore (WARREN ET AL., 1998) with both wave- and fluvial-dominated environments (GORTER AND GREY, 2012; MUNSON, 2016; SHERIDAN ET AL., 2018).

Three organic-rich intervals referred to as the A, B, and C shales, occur in the Amungee Member of the Velkerri Formation (MUNSON AND REVIE, 2018). In addition, high organic carbon contents have also been reported in the lower Kyalla Formation (JARRETT ET AL., 2019A; JARRETT ET AL., 2019B). Recent biomarker studies indicate that the organic matter in these sediments is derived from biomass dominated by bacteria with minor input from archaea and eukaryotes (JARRETT ET AL., 2019B). Total organic carbon (TOC) in individual shale units can exceed 12 wt%, with present day HI up to 800$mg_{HC}.g_{TOC}^{-1}$ (JARRETT ET AL., 2019A). The thermal maturity of the shales ranges from early mature at the margins of the basin to dry gas mature in the depocenters (REVIE, 2017A) where the maximum burial depth was estimated to reach 4000m (FAIZ ET AL, 2021). While older organic-rich rocks exist (e.g., Wollogorang Formation, SPINKS ET AL., 2016; KUNZMANN ET AL., 2020) the Velkerri and Kyalla formations are interpreted to be the source of the world's oldest recovered oil (CRAIG ET AL., 2013).

3. Dataset and methods

3.1. Data

Data from 32 wells were studied to reconstruct the stratigraphic architecture of the Velkerri-Kyalla interval. Among these wells, 25 intersected the Velkerri Formation, 16 intersected the Moroak

Sandstone and 19 intersected the Kyalla Formation (Supplementary Table 1). The available Gamma-Ray (GR) logs were loaded in EasyTrace, a well-log interpretation software distributed by BeicipFranlab, allowing for the creation of correlation panels. In addition to the GR logs, cored intervals from eight wells were studied for facies descriptions (Supplementary Table 2).

The Beetaloo Basin chemostratigraphic zonation scheme was defined internally by Chemostrat Pty Ltd on offset legacy wells with available elemental data from the greater McArthur area (CHEMOSTRAT AUSTRALIA, 2014, 2016; ORIGIN ENERGY RESOURCES LTD, 2015A, 2015B, 2016; COX ET AL., 2016; MUNDAY, 2020; MUNDAY AND FORBES, 2020). The wells correlated into this scheme include Amungee NW-1, Beetaloo W-1, Kalala South-1, McManus-1, Shenandoah-1, Alexander-1, Scarborough-1, Lady Penryn-1 and Altree-2. The elemental data (both major and trace elements) used for the chemostratigraphic correlation across these wells were derived from multiple operators using a range of XRF instruments (both calibrated handheld XRF and laboratory XRF), as well as Inductively Coupled Plasma - Optical Emission Spectrometry (ICP-OES), and Inductively Coupled Plasma - Mass Spectrometry (ICP-MS) analytical techniques.

Chemostratigraphy relies on the study of the geochemical variation in sedimentary rocks, typically being variable and sensitive to subtle shifts in provenance region or mechanisms of deposition (e.g. seawater and organic matter interaction). Successions that appear lithologically uniform often record differences related to the geochemistry of their mineral components or related to the abundance and proportions of accessory minerals, such as heavy and clay minerals, some of which have very distinctive trace element contents. Chemostratigraphy, therefore, results in the definition of zones with similar geochemical signatures and their correlations at various scales, analogous to a lithostratigraphic hierarchical scheme.

3.2. Methods

3.2.1. Sedimentary and well log facies

High-resolution images of cores, part of Hylogger datasets, were accessed through the AuScope portal (portal.auscope.org). This enabled the description of 2430 m of core distributed across eight wells. Sedimentological descriptions were carried out at the 1:200 scale, focusing on the identification of sedimentary structures and textures to define a facies model (*sensu* WALKER, 1992). As not all wells cored the Velkerri, Moroak and Kyalla formations, we integrate our facies descriptions with well-log patterns (*sensu* POSAMENTIER AND ALLEN, 1999), placing particular focus on the GR logs (e.g., CROMBEZ ET AL., 2016). GR logs were the most commonly acquired log type during the 40 years of drilling the wells. In the Velkerri-Kyalla interval, the mineralogy mostly reflects terrigenous material with very little carbonate content observed (REVIE, 2017A). Assuming the GR values approximate the abundance of K-rich micas mostly present in fine-grained material in the Velkerri-Kyalla interval, this log can be used to distinguish the proximal, more coarse-grained, sand-rich environments from the fine-grained, distal part of the sedimentary system. GR logs can also help to identify organic-rich marine intervals that are likely to be enriched in uranium.

3.2.2. Sequence stratigraphy

We reconstructed the stratigraphic architecture of the Velkerri-Kyalla interval along two 2D sections (Figure 1). Using sedimentological descriptions and GR logs to understand the distribution of sedimentary environments and to identify stacking patterns, we interpreted the sequence

stratigraphic evolution following a model-independent approach (*sensu* CATUNEANU ET AL., 2009, 2011; CATUNEANU, 2019). We focused on shoreline trajectories (HELLAND-HANSEN AND MARTINSEN, 1996; HELLAND-HANSEN AND HAMPSON, 2009) that resulted in the development of different stratigraphic surfaces and systems tracts, and followed the terminology defined by HUNT AND TUCKER (1992) AND HELLAND-HANSEN AND GJELBERG (1994). The present work aims to propose a 3D stratigraphic framework for this Mesoproterozoic hydrocarbon play, and to integrate this framework with the available chronostratigraphic and chemostratigraphic datasets. The sparse data set and poor age control means we simply assume that the observed deepening and shallowing trends are the consequence of transgressions and regressions and that the paleo-shoreline moved synchronously across the basin. Based on these interpretations it is implied that the identified transgressions and normal and forced regressions were synchronous. Indeed, in this case study, we cannot identify with confidence the coeval deposition of transgressive and normal or forced regressive systems tracts resulting from the spatially different sediment supplies or local structural movements.

4. Results

4.1. From cores to well logs

4.1.1. Sedimentary facies and environments

Based on the sedimentary facies identification criteria (Figure 3), four main facies associations were identified from the core descriptions (E1 to E4, Figure 4). It is noted that the limited quantity of data meant it was not possible to consistently distinguish wave- from fluvial- dominated areas (*sensu* AINSWORTH ET AL., 2011). Therefore, we group delta-front and foreshore environments in "E1: fluvial-influenced foreshore" environments, and shorefaces and pro-deltas in "E2: fluvial-influenced shoreface" environments. Two other environments are distinguished: turbiditic (E3) and offshore transition to offshore (E4). Here, we chose the wave denomination over the fluvial denomination because of the lack of observed unidirectional current structures and the abundance of wavy and tangential bedded strata , which are interpreted as the basin being wave-dominated and fluvial-influenced.

The fluvial-influenced foreshore environments (E1) are composed of planar-bedded, light grey to beige, fine-grained sandstone and siltstone. They preserve cross-bedding (Figure 3B), sometimes sub-massive (Figure 3A), or slightly wavy-bedded (Figure 3C). They are often marked by an erosional base with gravel lags (Figure 4). The planar- to cross-bedded sandstones are interpreted to reflect deposition in shallow marine environments, either in foreshores or upper shorefaces (WALKER AND PLINT, 1992) or in reworked sand bars (BHATTACHARYA AND WALKER, 1992). The large number of erosive surfaces and lags likely reflect storm or fluvial events on the margin.

Figure 3: Sedimentary facies from cores intersecting the Velkerri-Kyalla interval. A. Sub-massive sandstone; B. Cross-bedded sandstone, C. Wavy-bedded sandstone; D. Heterolithic sandstone and shale with synaeresis cracks; E. Heterolithic, sandstone and shale with synaeresis cracks and tangential bedding; F. Heterolithic, wavy-bedded sandstone and shale with synaeresis cracks and tangential bedding; G. Heterolithic, wavy- to planar-bedded sandstone and shale with fining-upward trends and erosive surfaces; H. Heterolithic, wavy- to planar-bedded sandstone and shale with unidirectional current ripples and erosive surfaces; I. Heterolithic, planar-bedded sandstone and shale; J. Heterolithic, wavy-bedded sandstone and shale; K. Massive to planar-bedded shale.

The fluvial-influenced shoreface environments (E2) are composed of wavy bedded, light to dark grey, heterolithic siltstone and shale. In this environment, fining-upward cycles (cm- to m-scale) preserving synaeresis cracks (Figure 3 D. and E) and tangential bedding (Figure 3 E and F) are common (Figure 4). The occurrence of fining-upward cycles, wavy bedding, and the heterolithic deposits is interpreted to be controlled by fair- and storm-weather wave oscillatory currents (DUMAS AND ARNOTT, 2006; SUTER, 2006). Furthermore, it is likely that the variation in the river flow regime affected the grain size of the sediments delivered to the basin, explaining the heterolithic nature of this environment. Synaeresis

cracks are interpreted to reflect the mixing of fresh and seawater (PLUMMER AND GOSTIN, 1981), attesting the presence of rivers delivering fresh water to the system.
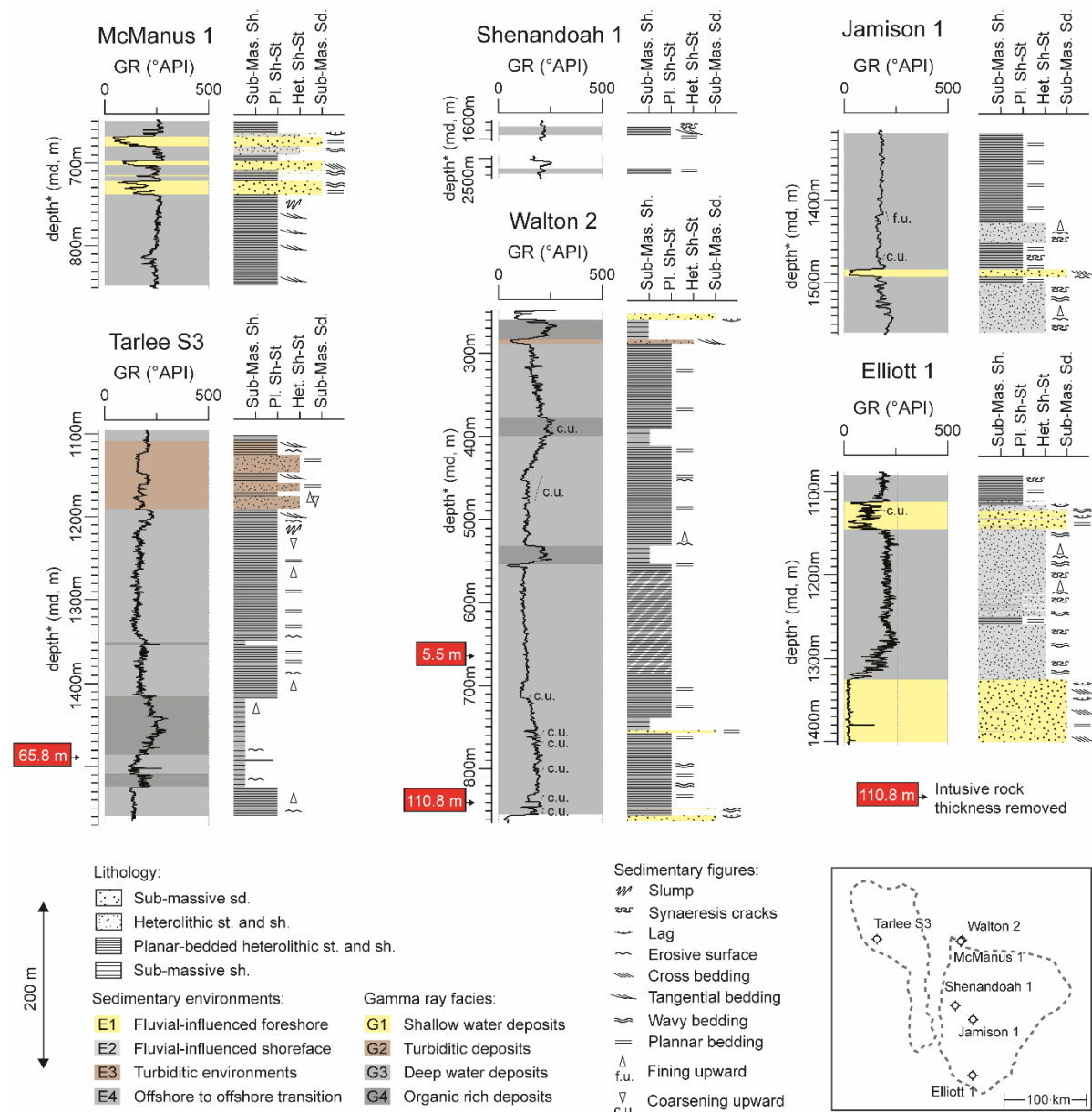
Figure 4: Synthetic facies description from studied drill cores. Identified facies reflect wave- to fluvial-dominated sedimentary environments. At the scale of the descriptions, and with the data available, no tide-dominated deposits were identified.

The turbiditic environments (E3) are composed of heterolithic planar-bedded, dark to light grey siltstone (Figure 3 I). Fining- and coarsening-upward trends can be present (Figure 3 G), as well as rare current ripples (Figure 3 H). These sediments are often surrounded by planar-bedded, dark grey shale and fine-grained siltstone with tangential bedding (Figure 4). In this facies, the planar-bedded siltstones are interpreted to represent distal lobe deposits formed on the shelf (BOUMA, 1964; WALKER, 1992). The fining-upward trends in the siltstones, together with the tangential bedding preserved in the shales surrounding the coarser interval, likely reflect the episodic evolution of the system controlled by periods of a higher flow regime in the river system feeding the basin.

Offshore transition to offshore environments (E4) are composed of planar-bedded to massive shale and fine-grained siltstone (Figure 3 K). Minor erosive surfaces, tangential bedding, fining upward and wavy-bedded (Figure 3 J) intervals are often present while synaeresis cracks are rare. Here, the planar bedding is attributed to hyperpycnal flows settling. Rare tangential bedding is interpreted to either reflect turbidite flows or storm-induced currents (DUMAS AND ARNOTT, 2006). The occurrence of small reactivation surfaces, or erosive surfaces, are also interpreted to be related to episodic storm activity or unidirectional currents (MACQUAKER ET AL., 2010). The massive, dark grey to black facies is interpreted to represent the deepest part of the sedimentary system and to reflect mainly pelagic settling below the storm-wave base (STOW AND PIPER, 1984; STOW ET AL., 2001).

Overall, the Velkerri, Moroak and Kyalla formations represent wave-dominated environments ranging from foreshore, upper and lower shoreface, to offshore. In this wave-dominated framework, the offshore transition reflects environments between storm- and fair-weather-wave base, while the shoreface-foreshore boundary is placed at the base of the low tide level. Although wave-dominated, the occurrence of synaeresis cracks within the Moroak and the Kyalla formations indicates the mixing of fresh- and saltwater and therefore a fluvial influence. The interpretation of a fluvial-influenced depositional environment is further supported by the occurrence of gutters and unidirectional currents (WILSON ET AL., 2021) that confirm sediments were deposited in a fluvial-influenced environment with sediment flowing to a turbiditic system.

4.1.2. Sedimentary environment and well log facies

Using GR logs, we extend the interpretation of depositional environments to uncored wells intersecting the Velkerri, Moroak and Kyalla formations. Although environmental reconstructions based on well logs are less precise compared with core logging, shoreline shifts can be reconstructed by distinguishing four GR facies (G1 to G4, Figure 4). Shallow water deposits (G1) often present low GR values and either have a sharp base or are located above decreasing GR trends. These low GR values are interpreted to reflect the high abundance of coarse-grained content in E1 environments. Sharp bases are the result of sudden changes in the sedimentary environment, while the gradual decrease in GR values is interpreted as a coarsening-upward trend indicating shoreline progradation.

Turbidite deposits (G2) are marked by a blocky GR pattern alternating from medium to high GR values. This likely reflects shifts from silt-rich lobe deposits to the mud-rich levee and overbank deposits of E3. High GR values are typical for deep water deposits of GR facies G3 and present high-frequency variation that is likely linked to subtle lithologic changes in the lower shoreface (E2) to offshore (E4) deposits. Finally, the highest GR values occur in facies G4 representing the organic-rich black shales (from E4). In addition to the four GR facies, which represent different depositional environments, GR trends can be linked to transgressions and regressions. While a gradual increase of the GR values (over 10s of meters) is interpreted to reflect a transgressive period, a gradual decrease of the GR values (over 10s of meters) is interpreted to reflect a regressive trend.

4.2. 2D well correlations

Our study is based on two well sections, oriented east-west (E-W) and north-south (N-S). The E-W well section spans 466 km and comprises 15 wells (Figure 5). It extends from Broadmere-1 in the east to Sever-1 in the west. The second well section spans 348 km and also comprises 15 wells (Figure 6). It extends from Prince-of-Wales-1 in the north to Elliott-1 in the south. The top of the Moroak Sandstone is used as a datum in both sections, assuming it represents a pseudo-horizontal surface. As we aim to establish a quasi-chronostratigraphic framework, our correlations may diverge from the lithostratigraphic subdivision of this succession.

On the E-W section, unit 1 (equivalent to the Kalala Member of the Velkerri Formation, Figure 5) records significant deepening from the top of the underlying Bessie Creek Sandstone. The sediments of this unit were mainly deposited below the storm-wave base, interrupted by rare occurrences of shoreface deposits. Unit 1 records two transgressive-regressive cycles. The top of the second cycle was previously highlighted by HOFFMAN (2015) as a continuous marker across the basin, being the only carbonate-rich interval. Unit 2 is 150-250 m thick (equivalent to the Amungee Member; Figure 5) and records deep water deposition below the storm-wave base, with minor to no shoreface influence and rare turbidite deposits. This interval records three significant peaks in the GR log, which often show a 'Christmas tree' pattern, as indicative of there being a high uranium concentration in the sediment-starved intervals (CROMBEZ ET AL., 2020). The three high GR intervals match the definitions of the A, B, and C organic-rich shale intervals (MUNSON AND REVIE, 2018). The uppermost cycle generally represents the highest GR values and is inferred to record the highest concentration of fine material linked to the lowest sedimentation rate. We interpret this interval to represent the most distal part of the sedimentary system. Unit 3 (300-500 m, equivalent to the Wyworrie Member, Figure 5) comprises offshore to lower shoreface sedimentation. Siltstone beds are interpreted as thin, gravity-flow deposits. Above these, two transgressive-regressive cycles are recorded, although the abundance of turbidite deposits makes it more challenging to identify these cycles as clearly as those in unit 2. The thickness of the overlying unit 4 (Figure 5) varies significantly across the basin. It may reach almost 500 m in the east (where it is equivalent to the Moroak Sandstone) but thins to approximately 100 m in the west. This interval is mainly composed of shallow water deposits in the east, which gradually transition to deeper water deposits in the west. Two transgressive-regressive cycles are recorded in unit 4. Importantly, the transgressive parts are thinner compared to those in the underlying transgressive-regressive cycles. The overlying unit 5 (equivalent to lower Kyalla, ca. 250 m, Figure 5) records a significant deepening of the depositional environments at its base. At least one transgressive-regressive cycle is apparent. It comprises shoreface deposits in the east (equivalent to the Elliott sandstone member) and turbidite deposits in the west. Unit 6 is up to 550 m thick and truncated by a major erosional surface (YANG ET AL., 2020A). It mostly comprises deposits formed below the storm-wave base, arranged in two transgressive-regressive cycles.
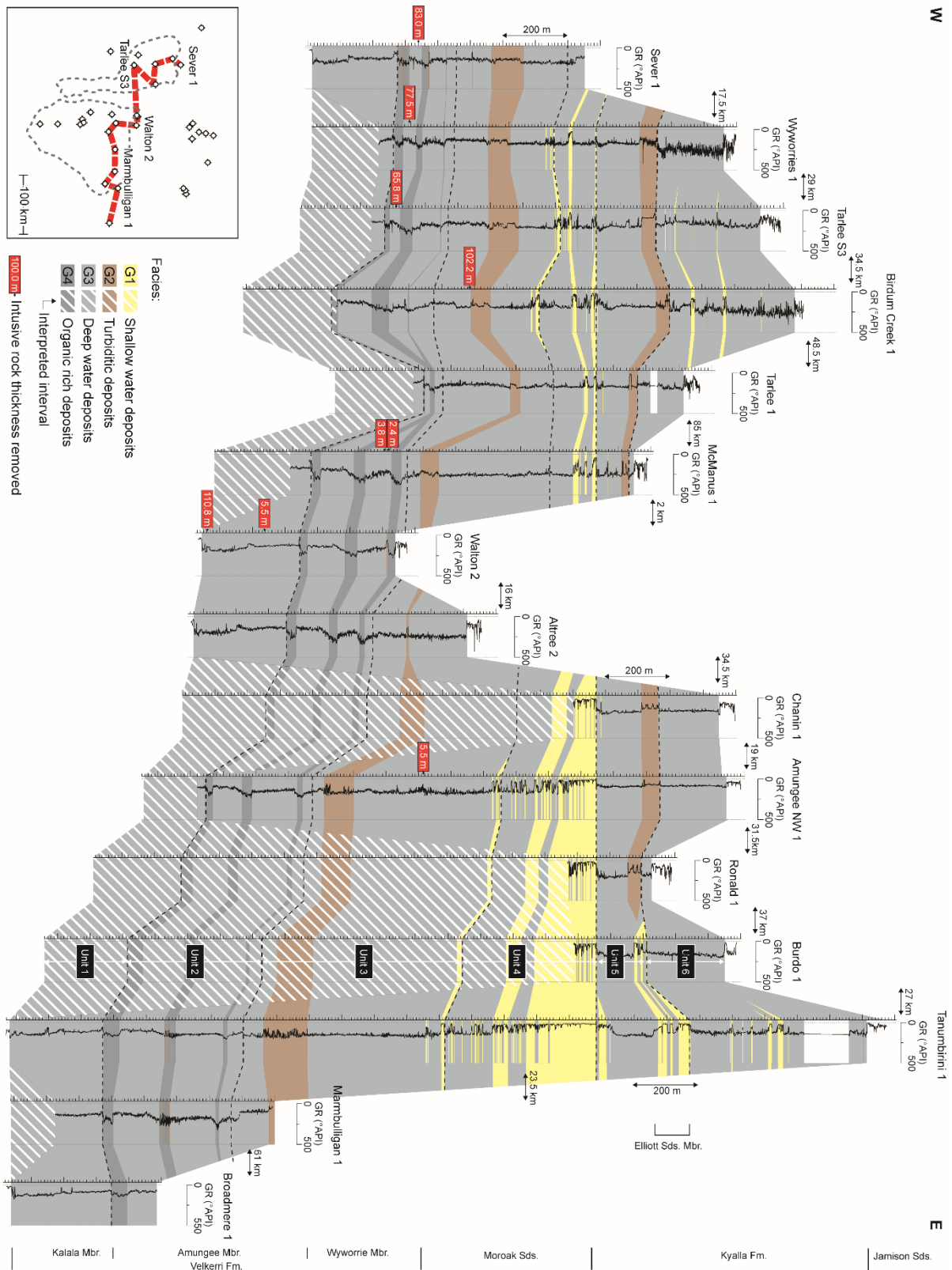
Figure 5: Interpreted facies distribution along a W-E well section. Note the thinning of the proximal deposit of the Amungee member toward the west, not accompanied by sudden changes in facies and thickness across the Daly Waters High (located between Birdum-Creek-1 and McManus-1).
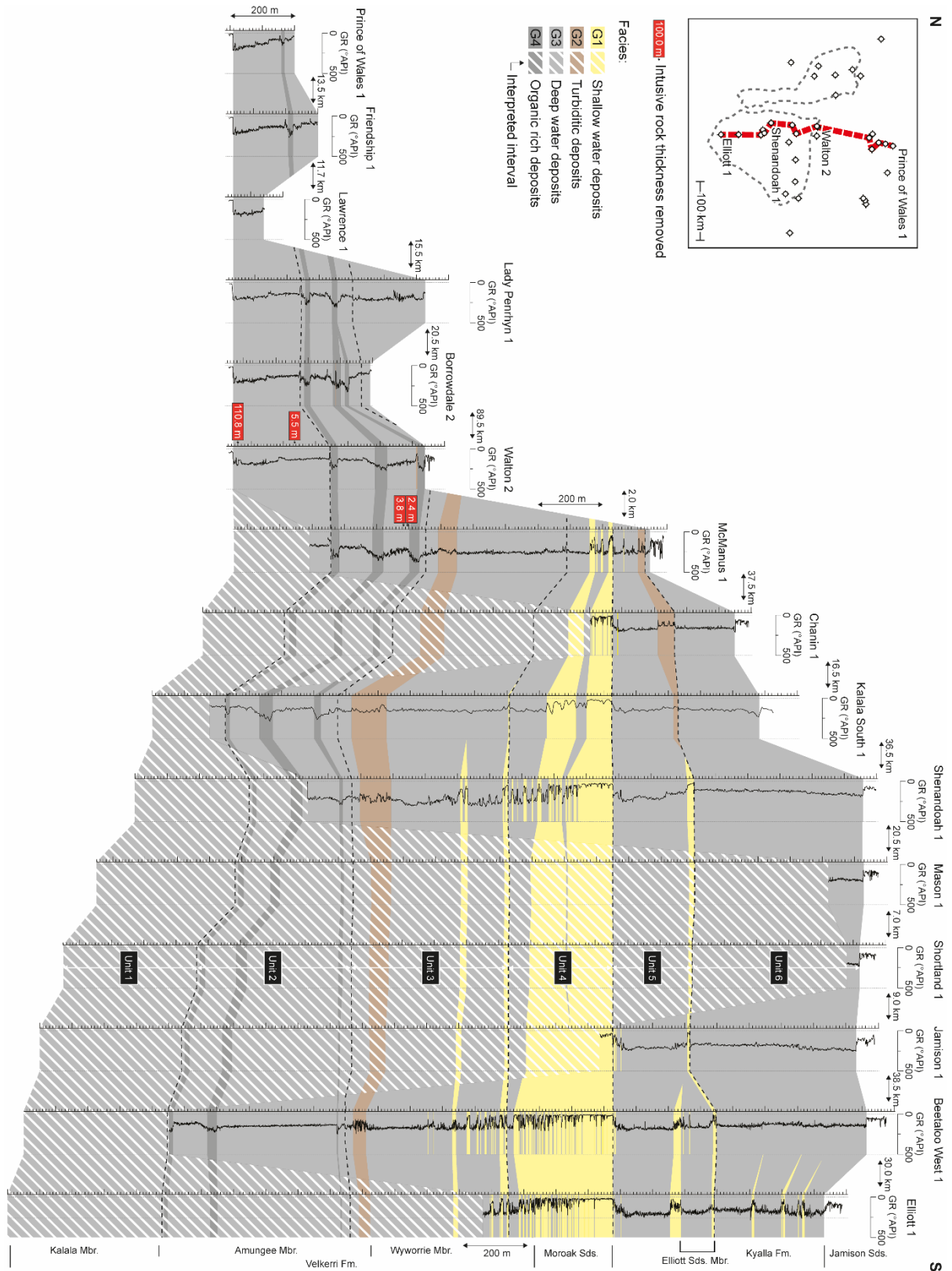
Figure 6: Interpreted facies distribution along an N-S section. Note the thinning of unit 2 (approximating Amungee Member) toward the north and onlapping of the uppermost shale (C shale) onto the middle shale (B shale) in the northern part of the basin.

The N-S section records a similar facies distribution as the E-W section (Figure 6). Unit 1 is only intersected in the north, where it records deposition below the storm-wave base with the rare occurrence of lower shoreface deposits. Comparable to the E-W cross-section (Figure 5), two

transgressive-regressive cycles are developed in unit 1 and a carbonate-rich interval occurs at the top of the second cycle (Figure 6). Unit 2 also preserves the three transgressive-regressive cycles observed on the E-W transect. In the central part of the basin (e.g., Kalala-South-1), this unit records three high GR intervals. The thickness of unit 2 is variable, measuring more than 600 m in the south, and thinning to ca. 150 m in the north. Importantly, the second and the third shale (B and C) merge in the northern part of the basin between Borrowdale-2 and Lady-Penrhyn-1. Just as along the E-W section, unit 3 is characterized by the occurrence of turbidite deposits and two transgressive-regressive cycles. Unit 4 records a facies shift from shallow water deposits in the south to deep water deposits in the north. The shallow water deposits thin from 300 m in Elliott-1 to less than 50 m in McManus-1 (Figure 6). These observations are similar to those made along the E-W transect, which also demonstrates thinning and deepening from east to west (Figure 5). Unit 5 again records significant deepening across the study area; however, in contrast to the E-W section, two transgressive-regressive cycles are preserved within this unit (Figure 6). The second cycle records a similar facies distribution as the one observed along the E-W transect, which we interpret as the Elliott sandstone member of the Kyalla Formation. Unit 6 mostly comprises offshore to lower shoreface deposits, arranged in two transgressive-regressive cycles. This unit reflects an overall deepening of the depositional environments.

5. Discussions

5.1. Stratigraphic architecture

An understanding of the 2D facies distribution along two transects allows us to relate the observed facies shifts to relative sea level variations. This in turn allows us to reconstruct the stratigraphic architecture of the shale play. In the greater McArthur Basin, regional unconformities interpreted to have formed in response to major tectonic events, bind the major sedimentary groups (**RAWLINGS, 1999**). These unconformities have previously been interpreted as 1st-order sequence boundaries (**KUNZMANN ET AL., 2020**). In our case study, this means the unconformities at the base and top of the Roper Group represent such 1st-order sequence boundaries. Lower rank sequences are nested within this 1st-order sequence (**CATUNEANU, 2019B**) and the identified sequences within the Velkerri, Moroak and Kyalla formations represent 2nd and lower order sequences.

5.1.1. Second-order stratigraphic evolution

As the stratigraphic architecture results from the complex interplay between sediment supply and accommodation, not all systems' tracts have to be developed and preserved in all locations across a sedimentary basin (**CATUNEANU, 2006, 2019A**). At the scale of the study (300-500 km), the 2nd-order sequence boundaries (SB) will be expressed as unconformable contacts. In the Beetaloo Sub-basin (i.e., 60 000km^2) the Bessie Creek Sandstone is unconformably overlain by the Velkerri Formation (**MUNSON, 2016**). The boundary between the Moroak and the Kyalla formations is an unconformable surface in the eastern part of the basin but becomes conformable in the western Beetaloo (Figure 5). The uppermost major unconformity in this study is the boundary between the deep water facies of the Kyalla Formation and the shallow water/continental facies of the overlying Jamison sandstone. This is the 1st-order sequence boundary developed at the top of the Roper Group, which is developed as an erosive surface and is interpreted to have removed several 100s of meters of stratigraphy (**YANG ET AL., 2020A**). Considering the characteristics of these three surfaces, the one at the top of the Bessie Creek Sandstone is interpreted to be 2nd-order. The unconformity at the top of the Roper Group, being

of 1st-order, will also bind a 2nd-order sequence (Figure 7 and Figure 8). This implies that the studied interval comprises one 2nd-order sequence that should include a major maximum flooding surface (MFS). In the Velkerri and Kyalla formations, several intervals were deposited below the storm wave-base and are characterized by high GR values and represent potential MFSs. Among these deep water deposits, unit 2 (A, B, and C shales from the Amungee Member) records a high organic content (WARREN ET AL., 1998; MUNSON AND REVIE, 2018; JARRETT ET AL., 2019B). This could be attributed to organic matter concentration in sediment starved environments related to increased distance from sediment sources (PASSEY ET AL., 2010), occurring at the maximum backstep of the sedimentary system. In detail, GR values are often higher in the C shale than in the A and B shales, which is interpreted as the effect of lower dilution of authigenic uranium by detrital particles (CROMBEZ ET AL., 2020). This surface has a basin-wide extent, and we interpret it as a 2nd-order MFS (Figure 7 and Figure 8). The underlying units 1 and 2 (Kalala and Amungee members, up to the C shale) represent a 2nd-order transgressive systems tract (TST), which is followed by a 2nd-order regression spanning the interval from the C shale to the sub-Jamieson unconformity. At this order, no downstepping is observable, which suggests that the 2nd-order regression recorded in units 3-6 (ca. Wyworrie Member, Moroak, and Kyalla formations) is normal and represents a 2nd-order highstand systems tract (HST). However, a 2nd-order forced regression should not be excluded and could be present below the erosional surface at the base of the Jamison sandstone. In this 2nd-order framework, the Jamison sandstone is interpreted as a lowstand systems tract (LST), being deposited in a continental (GORTER AND GREY, 2012), or shallow water setting (MUNSON, 2016), after a relative sea level drop that resulted in the erosion of the top of the Kyalla Formation. In the studied interval, besides the Jamison sandstone, no LST is identified in any other order. In this case study, 2nd-order SBs are expressed as a shift from "shallow water" regressive deposits to "deep water" transgressive units and the SBs are stacked with the transgressive surfaces (TS).

5.1.2. Third-order stratigraphic evolution

Within the 2nd-order sequences, a higher frequency of cyclicity is observed in the Velkerri, Moroak and Kyalla formations. Nested 3rd-order sequences will be bound by 3rd-order SBs, as well as 1st- and 2nd-order SBs already identified. While 2nd-order cyclicity implies basin-wide shoreline shifts, 3rd-order SBs in the Beetaloo are interpreted to record shifts of a few 10s of kilometres. This means that the 3rd-order SBs are expected to gradually change expression across the basin. A potential 3rd-order SB is the surface at the top of unit 1 (below the A shale). It represents an important facies shift from strata deposited above the storm wave-base to deep water facies. While this surface does not show evidence of erosion, its significant lateral extent (100s km) makes it a potential 3rd-order SB. Higher in the stratigraphy, the surface at the transition between units 4 and 5 (ca. Moroak and the lower Kyalla Formation) reflects a significant vertical facies change and is potentially erosive in the southern and eastern parts of the study area. In addition, the surface at the top of unit 5 (Elliott sandstone member; Figure 5 and Figure 6) is likely unconformable in the south and east but transitions into a conformable surface towards the north and west. As this surface also records an abrupt facies change in most parts of the basin, it is interpreted as 3rd-order SB. In summary, three 3rd-order SBs were identified in the studied interval, in addition to the 1st and 2nd-order SBs previously identified bracketing four 3rd-order sequences.

Figure 7: Stratigraphic architecture of the Velkerri-Kyalla interval along an E-W transect. Note on this figure the colours represent the 3rd*-order systems tracts, and the stratigraphic lines' strokes account for the different stratigraphic orders.*
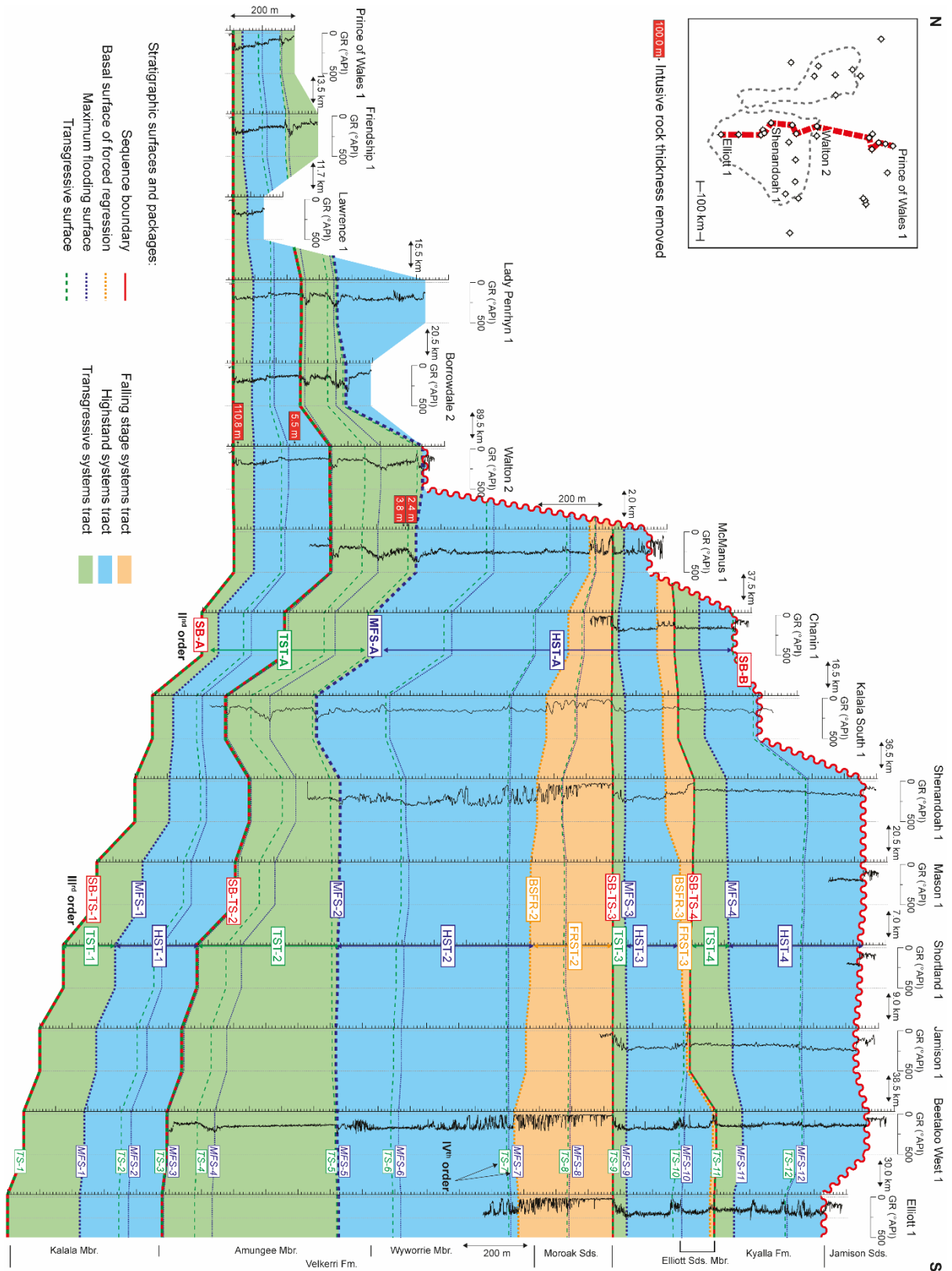
Figure 8: Stratigraphic architecture of the Velkerri-Kyalla interval along an N-S transect. Note on this figure the colours represent the 3rd-order systems tracts, and the stratigraphic lines' strokes account for the different stratigraphic orders.

The oldest 3rd-order sequence comprises two transgressive-regressive cycles. Of these two cycles, the first one often records a surface with the highest GR values within this sequence. We interpret this surface as the corresponding first 3rd-order MFS. No other sequence stratigraphic surface is

identifiable in the available data set for this sequence; therefore, we divide this 3rd-order sequence into a HST overlying an TST.

The second 3rd-order sequence contains the 2nd-order MFS that is also interpreted as a 3rd-order sequence MFS. In the upper part of the sequence, the shallow water deposits that constitute unit 4 (ca. Moroak Sandstone) can either be interpreted as being a highstand normal regressive or a forced regressive. In the case of a highstand normal regression, the rising relative sea-level would generate accommodation on the margin of the basin, which would likely be filled by backshore and continental deposits. Neither our study nor previous work on the Moroak Sandstone (POWELL ET AL., 1987; MUNSON, 2016) report such sedimentary environments, with the shallowest parts of unit 4 (ca. Moroak Sandstone) being described as tidal flat deposits. The absence of continental deposits in the known extent of the Moroak Sandstone suggests that accommodation was not created at the basin margin. These observations are more compatible with a forced regression and downstepping of the shoreline (CATUNEANU, 2006). A basal surface of forced regression (BSFR) is therefore interpreted at the base of unit 4 (ca. Moroak Sandstone). It separates an HST present in unit 3 (above the C shale) and a falling stage systems tract (FSST) present in unit 4 (ca. Moroak Sandstone) from the top of the second 3rd-order sequence (Figure 7 and Figure 8). While the observed sedimentary environments are compatible with a forced regression, the absence of a significant erosion surface to the east and south of the basin suggests that the relative sea-level fall was of limited amplitude.

Above unit 4, the third sequence records two transgressive-regressive trends. The second one appears poorly preserved along the eastern part of the basin (Figure 5). In this sequence, the deepest sedimentary environments are observed 10s of meters above the base of the sequence and are interpreted as MFSs. Towards the south and east of the basin, the top of the sequence comprises shallow water deposits that progressively transition into gravity flow deposits towards the west (equivalent to the Elliott sandstone member). In detail, the GR log often records a sharp drop, which reflects a sudden basin-ward shift of the shoreline (CATUNEANU, 2019A). This is likely accompanied by the truncation of the underlying strata, explaining the poor preservation of the second transgressive-regressive cycle in the eastern part of the basin (Figure 5). We interpret this sudden facies shift as forced regression, with its basal surface placed at the GR drop in the east and south and beneath the gravity flow deposits in the west. Alternatively, the unit 4 interval may be either a highstand or lowstand normal regression. However, this would imply that during the deposition of the sand-rich interval the relative sea-level was slowly rising, favouring the accumulation of continental deposits on the edges of the basin. As we did not identify any non-marine facies in the Elliott sandstone member, the highstand or lowstand normal regression interpretations seem unlikely.

The uppermost 3rd-order sequence recorded in the studied interval is truncated by the 1st-order sub-Jamison sequence boundary. This sequence comprises two well-developed transgressive-regressive cycles across the basin. In the southern and eastern parts of the basin, multiple prograding deposits occur that are difficult to identify in other parts of the basin. In the west, the GR log shows progressively increasing values, which we interpret as a fining-upward trend. Identifying an MFS is more challenging than in the underlying 3rd-order sequences. Because of the occurrence of multiple coarse-grained, prograding deposits in the upper part of this sequence, we interpret the MFS to be located at the end of the first deepening cycle. In this sequence only two systems tracts are identifiable, a TST and an HST.

In the third order, similarities exist with the stratigraphic architecture suggested by ABBOTT AND SWEET (2000). Our basal sequence boundary (SB1) and the SB3 respectively correspond to the base and top

of their Veloak sequence, while the SB3 and the topmost SB5 respectively correspond to the base and top of their Shermi sequence. By adding more wells intersecting the Velkerri-Kyalla interval, we are able to refine previous work on the stratigraphy of these formations and identify additional sequences previously not identified.

5.1.3. Fourth-order stratigraphic evolution

The available facies and GR data permit the identification of high-frequency cyclicity nested within the 3rd-order sequences of the Velkerri, Moroak and Kyalla formations. These cycles are between 100 m (in the west and north) and 250 m thick (in the south and east), and we interpret them as 4th-order sequences (CATUNEANU, 2019B). Although clearly identifiable, the available data does not allow the identification of stacking patterns necessary to divide the regressive part into lowstand, highstand, and forced regressive deposits (*sensu* HUNT AND TUCKER, 1992, and HELLAND-HANSEN AND GJELBERG, 1994). Therefore, we use the framework proposed by JOHNSON AND MURPHY (1984), only distinguishing two surfaces: maximum regressive surfaces (MRS) and MFS. These surfaces are used to distinguish regressive systems tracts (RSTs) and TSTs. Twelve 4th-order sequences can be identified from our data set. In addition, a thick interval of turbidite deposits, most likely representing another 4th-order regressive event, suggest that a 13th T-R cycle may have occurred in unit 3 (ca. Kalala Member).

5.2. Chronostratigraphic framework

Previous work on the Velkerri, Moroak and Kyalla formations provided a number of different age constraints for these units (ABBOTT ET AL., 2001; KENDALL ET AL., 2009; YANG ET AL., 2018, 2019). Recently, YANG ET AL. (2018) suggested that the Velkerri and Moroak formations were deposited between 1349 Ma and 1320 Ma, while the Kyalla Formation must be younger than 1313 ± 47 Ma and older than the maximum depositional age of 959 ± 18 Ma of the overlying Jamison sandstone. The integration of these available age constraints into our sequence stratigraphic framework allows us to better understand the age and duration of the studied stratigraphic interval. Without integration, the available ages suggest high sedimentation rates for the Velkerri-Moroak interval; for example, 110 m x Ma^{-1} for Tanumbirini-1 and 90 m x Ma^{-1} for Amungee-NW1 (assuming the uncompacted thickness to have been 1.8 times higher than the current; FOWLER AND YANG, 1998). Organic-rich rocks generally form under low sedimentation rates (< 50 m x Ma^{-1}, TYSON, 2001). Considering that the primary productivity in the Proterozoic was generally low (CROCKFORD ET AL., 2018), the sedimentation rates in the Velkerri-Moroak interval may have been less than 50 m x Ma^{-1}. However, they could have also been close to modern values, considering that individual Proterozoic basins are reported to have had higher organic matter burial rates (HODGSKISS ET AL., 2020).

By integrating the detrital zircon geochronology data from previous studies (YANG ET AL., 2018, 2019; Supplementary Table 2) into our stratigraphic architecture, we were able to construct a chronostratigraphic framework. To do so, we selected samples with a concordance of ≥ 95% between ^{206}Pb/^{207}Pb and ^{206}Pb/^{238}U ages. As recommended by COPELAND (2020), we only consider the youngest zircon age to represent the maximum depositional age.
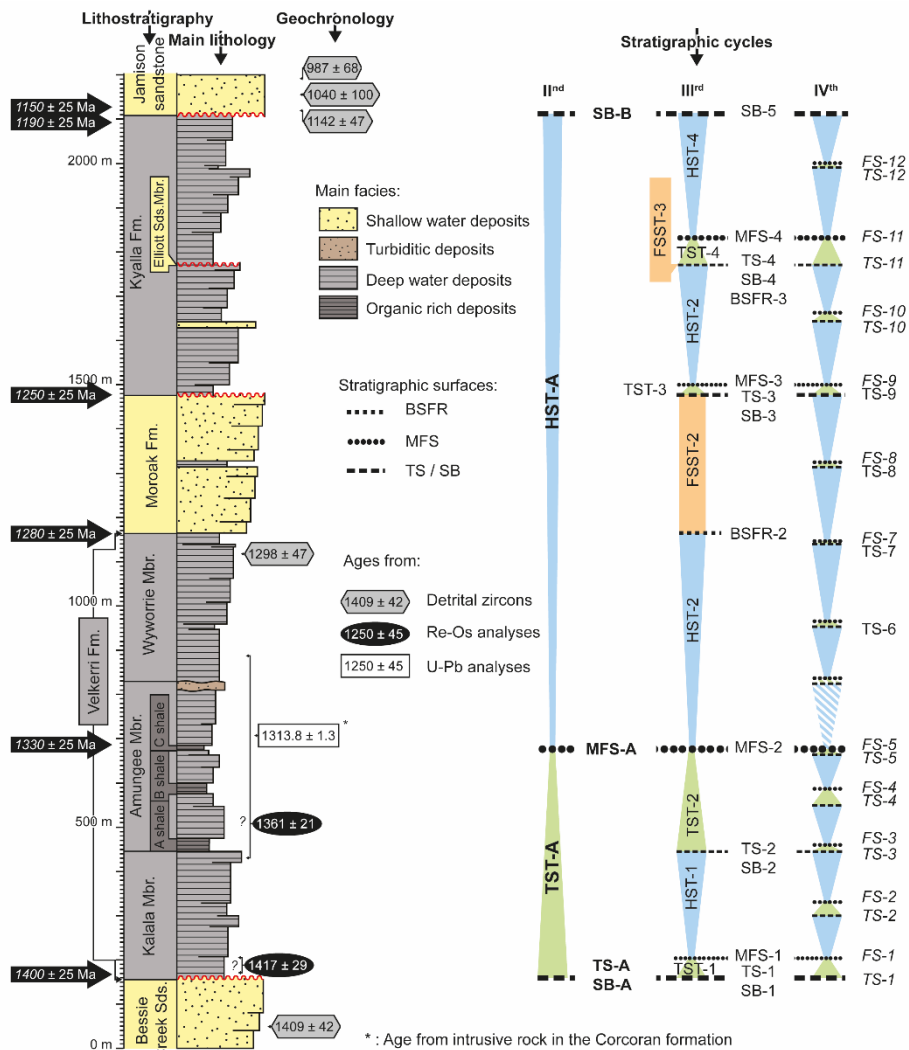
Figure 9: Lithostratigraphic, chronostratigraphic, and sequence stratigraphic framework of the studied interval (data from ABBOTT ET AL., 2001; KENDALL ET AL., 2009; YANG ET AL., 2018, 2019). Note this is a composite section based on wells Altree-1, McMannus-1, and Elliott-1. On this figure, the ages in the black arrows are interpreted from all chronostratigraphic data available. The ± 25 Ma represent 10% of the Velkerri-Kyalla interval deposition.

When integrated into our stratigraphic framework, only five of the 20 reported samples present a maximum depositional age younger than the underlying strata. As shown in Figure 9, integrated with available Re-Os ages, only three samples are considered to provide significant insights into the depositional ages of the Velkerri, Moroak and Kyalla formations. A zircon was analysed from the Jamison sandstone that yielded a maximum depositional age of 1142 +/- 47 Ma. This indicates that the underlying Kyalla Formation was likely deposited prior to ca. 1150 Ma. At the top of the Wyworrie Member, a zircon yielding a maximum depositional age of 1298 ± 47 Ma suggests that the transition from the Velkerri Formation to the Moroak sandstone occurred around 1280 Ma. Finally, a zircon from the Bessie Creek Sandstone yielded a maximum depositional age of 1409 ± 42 Ma, implying that the base of the Velkerri Formation is not older than ca. 1400 Ma. In addition to the selected detrital zircons, available Re-Os constraints from KENDALL ET AL. (2009) collected from well Urapunga 4 to the north of the Beetaloo Sub-basin provide a Re-Os age of 1417 ± 29 Ma at the base of the Velkerri Formation, which is compatible with the interpreted depositional age of ca. 1400 Ma for the base of this interval. Another Re-Os age indicates an age of 1361 ± 21 Ma for the uppermost organic-rich interval of the Velkerri Formation. This is compatible with a maximum depositional age of 1280 Ma for the top of the Velkerri Formation.

Previous work often refers to a U-Pb intrusive age to constrain the minimum depositional age for the Velkerri and Kyalla formations. However, these ages are not utilized in this study as they are derived from outcropping units to the north of the study area (ABBOTT ET AL., 2001), or intrusive rocks located in the underlying strata (BODORKOS ET AL., 2020). Thus, they do not provide direct calibration of the depositional age of the units in the subsurface of the Beetaloo.

The geochronological framework indicates that the Velkerri Formation was deposited over a period of ca. 120 m.y. This suggests an average duration of ca. 15 m.y. for each of the eight fourth-order transgressive-regressive cycles. Assuming a similar duration for the cycles in the Moroak sandstone and the Kyalla Formation gives an age of ca. 1250 Ma for the boundary between the Moroak sandstone and Kyalla Formation, and an age of ca. 1190 Ma for the top of the Kyalla Formation. Using the presented chronostratigraphic framework, sedimentation rates computed for both the Velkerri and Moroak formations, respectively, are 21.26 m x Ma^{-1} for Tanumbirini-1 and 17.4 m x Ma^{-1} for Amungee-NW-1. These sedimentation rates are consistent with values expected for Proterozoic organic-rich shales (< 50 m x Ma^{-1}). They are also within the same order of magnitude as a recent estimate of 40 m x Ma^{-1} (post-compaction) for the Velkerri Formation based on Milankovitch cyclicity infers (MITCHELL ET AL., 2020).

Our chronostratigraphic framework allows us to calculate the duration of sequences of different hierarchical ranks, assuming the transgressive-regressive cycles have a constant cyclicity. The 2nd-order sequence represents a duration of at least 210 m.y. Assuming 300 m of sediment were eroded at the top of the Kyalla Formation (FAIZ ET AL., 2021), which represents approximately two transgressive-regressive cycles. It places the end of the Kyalla deposition at ca. 1160 Ma. This is compatible with the youngest zircons analysed in the lower Jamison sandstone (Figure 9). The 3rd-order sequences span on average 52.5 m.y., with the second sequence recording the longest duration (105 Ma) and the first sequence recording the shortest duration (30 Ma). In summary, the 4th-order sequences in the studied stratigraphic interval are ca. 15 m.y. long; the 3rd-order sequences between 50 and 100 m.y long; and, the 2nd-order sequences at least 200 m.y. long. These sequence durations are systematically longer than the average ranges presented by a recent study on the cyclicity of the sedimentary records globally (300 yr to 0.1 m.y. for 4th order, 10000 yr to 3 m.y. for 3rd order, and 0.5 to 30 m.y. for 2nd order; CATUNEANU, 2019B). Since the data presented in CATUNEANU (2019B) largely stem from Phanerozoic basins, this may indicate different controls on sequence formation in the mid-Proterozoic.

Erosion rates are mainly controlled by the uplift rates that control the slope (SCHALLER ET AL., 2001; MONTGOMERY AND BRANDON, 2002) and the climate that will drive the expression of chemical and mechanical erosion processes (SUMMERFIELD AND HULTON, 1994; MOLNAR, 2004; JIONGXIN, 2005). At the time of deposition of the studied interval, the atmosphere and the biosphere were significantly different from today (LYONS ET AL., 2014), which suggests a different, poorly quantified control of the climate on the erosion rates. Present day estimations of erosion rates show values of up to 10 mm x yr^{-1} (10 000 m x Ma^{-1}) and suggest a strong relationship with topography (MONTGOMERY AND BRANDON, 2002) and the uplift rates (CYR ET AL., 2010). In the Proterozoic, the topography around the basin was probably low as the closest mountain ranges were 250 km south of the basin (YANG ET AL., 2020B). Because of this low topography and the absence of land plants, we interpret the erosion rate to be in the lower part of the present-day range, i.e. less than 0.10 mm.yr^{-1} (100 m.Ma^{-1}). This suggests that the erosion at the top of the Kyalla Formation took place in a few million years, which agrees with the maximum depositional age determined from zircons found in samples from the lower Jamison sandstone.

5.3. Controls on stratigraphic evolution and regional implications

5.3.1. Sediment sources and links to chemostratigraphy

The reconstructed facies distribution provides important information on the directions from which sediments were supplied. All the units thin towards the north and west. In addition, shallow water deposits are the predominant facies in the wells that intersect the southern and eastern part of the Moroak Sandstone (e.g., Elliott-1 and Tanumbirini-1) and pinch out towards the north and west (e.g., Tarlee-S3). In the Elliott sandstone member of the Kyalla Formation, turbidite deposits occur in the western part of the basin and are interpreted to be temporally equivalent with the shallow water deposits in the east (e.g., Tanumbirini-1). These observations indicate that the proximal part of the sedimentary system was located in the southeast and the basin deepened to the northwest. Furthermore, no significant changes in sediment supply direction occurred during the deposition of the Velkerri to Kyalla formations. This contrasts with the interpretation of YANG ET AL. (2020A) who suggested that sediments were partly delivered from the north.

Further constraints on sediment sources are provided by integrating the chemostratigraphic framework from MUNDAY AND FORBES (2020) with our stratigraphic architecture (Figure 10). A total of five chemo-sequences (S0-S4) were distinguished and have been further subdivided into chemo-packages based on the variability of elemental composition. The relative elemental abundance is interpreted to reflect variations in sediment provenance and depositional processes, as well as the environment of deposition and diagenetic alteration.

In the Velkerri Formation, the transition from the first to the second 3rd-order sequence coincides with the transition from the first to the second chemo-sequence, which is interpreted as a distinct change in sediment provenance. The first sequence is characterised by relatively high Zr content, most likely caused by increased zircon abundance. The second sequence has more mafic characteristics, indicated by an increase in ratios such as Ti/Nb and Ti/Th ratios and is, in addition, also enriched in phosphorus (COX ET AL., 2016; MUNDAY AND FORBES, 2020). A potential source was located in the Mount Isa region (YANG ET AL., 2018). The second shift in geochemical composition is recorded above the C shale (Figure 10). This shift reflects a return to a more felsic source (MUNDAY AND FORBES, 2020) located to the east of the basin (YANG ET AL., 2019).
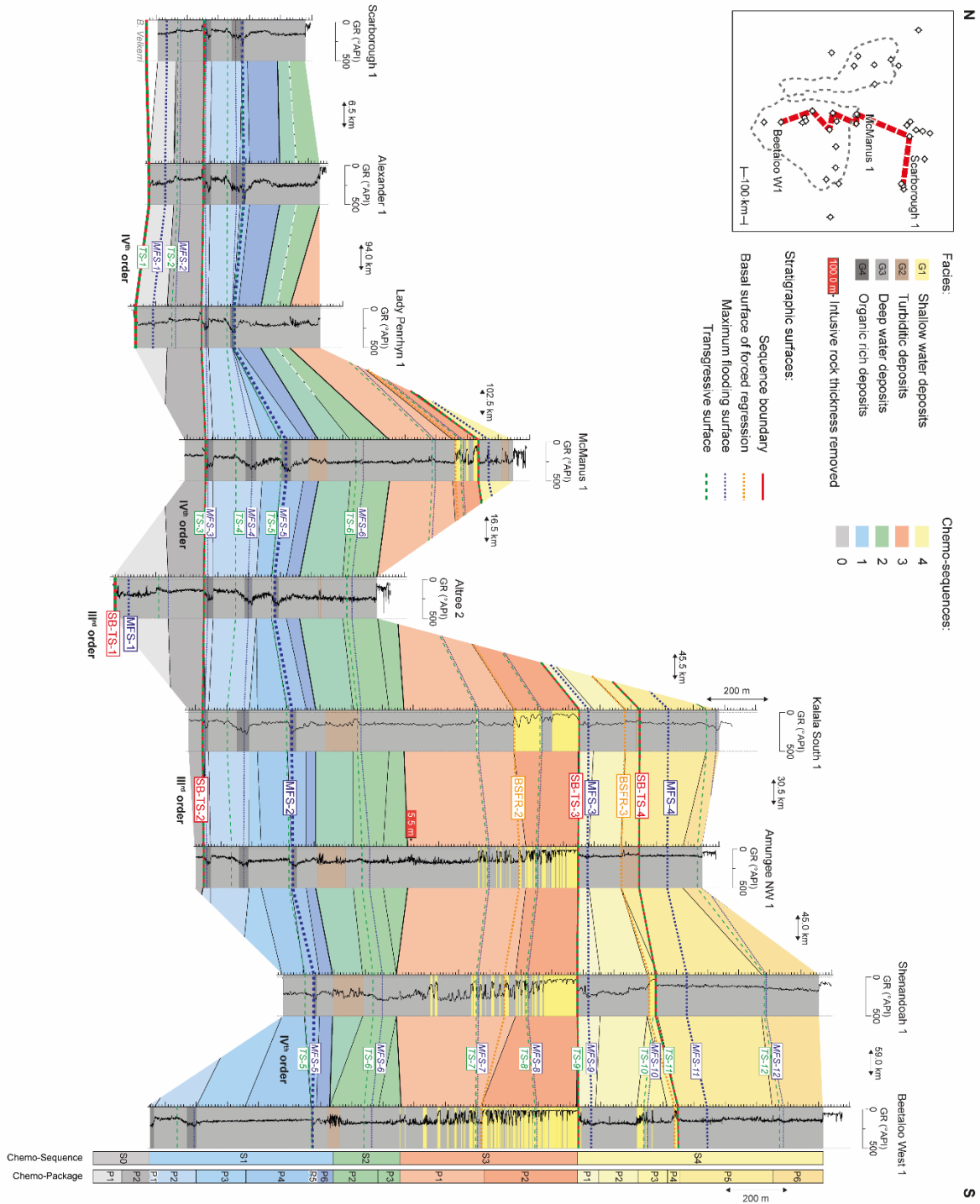
Figure 10: Stratigraphic and chemostratigraphic frameworks of the Velkerri, Moroak, and Kyalla formations. The chemostratigraphic packages are from MUNDAY AND FORBES (2020). Note the different colours relate to different chemo-sequences.

The transition from the Amungee to the Wyworrie Member is characterised by a shift from relatively high Na concentrations to high K concentrations, reflecting a switch from plagioclase-dominant feldspars to potassium-rich feldspars, as well as a significant and sustained increase in Zr concentration. It is important to note that this return to a more felsic source coincides with the end of the deposition of organic-rich units. Changes in elemental composition at the base of the Moroak

Sandstone (S2 to S3) are considered to represent a change in facies - from pro-delta to delta-front - rather than a change in sediment provenance. It is interpreted to be related to the occurrence of a 3rd-order forced regression. The shift from chemo-sequence 3 to 4 is commonly marked by the occurrence of an ironstone (Sherwin Member) on top of the Moroak Sandstone displaying Fe-rich lithologies. The overlying Kyalla Formation is itself characterised by its high Rb/Al ratio and coincides with a shift in detrital zircon provenance (YANG ET AL., 2019). The detrital zircon data were interpreted as indicative of a provenance shift from the east (e.g., Mount Isa region) to the south (e.g., Arunta region, YANG ET AL., 2019). However, detailed chemostratigraphic analyses highlighted numerous similarities between chemo-sequence 2 and 4 (MUNDAY AND FORBES, 2020), suggesting that this shift reflects a change in the depositional environments but maintains similar source compositions. Furthermore, the single chemo-sequence identified in the Kyalla Formation is consistent with the absence of a northern source region that would likely have had a different geochemical signature.

Chemo-package and chemo-sequence boundaries often coincide with surfaces of sequences of stratigraphic significance. This suggests that, at the scale of the study, the factors that controlled the sequence stratigraphic architecture also affected the chemostratigraphy. The good correlation between the interpreted sequence stratigraphy and chemostratigraphy in the basin corroborates that both datasets are complementary. Chemostratigraphic data are very powerful for reinforcing sequence stratigraphic interpretations in areas and intervals of lower confidence.

5.3.2. Structural framework and relative sea-level variations

The Daly Waters High (Figure 1) presently splits the sub-basin into two depocenters (eastern and western depocenters) and was previously interpreted as a topographic high during the Proterozoic (YANG ET AL., 2020B). Stratigraphic observations from wells on either side of this structure (e.g., Tarlee-S3 and McManus-1) do not indicate significant thickness or facies variations during the deposition of units 2-6 (ca. the Amungee and Wyworrie members of the Velkerri Formation, and the Moroak sandstone and Kyalla Formation). This suggests that the Daly Water High did not affect sediment dispersal at the time of deposition and only became a prominent structural feature in the basin after the deposition of the studied interval. However, this does not imply there were earlier or later structural reorganisations along the Daly Water High in the basin. In fact, significant thickness variation between the Tarlee-1 and Birdum-Creek-1 wells suggests there was a local bathymetric high within the eastern depocenter during the deposition of the A, B and C shale. While the available data are not sufficient to accurately locate all the small structural features, the thinning of the unit 2 (equivalent to the Amungee Member) in Tarlee-1 suggests that local structural movements may have occurred within the two depocenters. Similar observations can be made in the northern part of the basin, where stratigraphic correlations, supported by chemostratigraphy (MUNDAY AND FORBES, 2020), indicate the stratigraphic pinch out of the interval usually separating the B and C shales. The B and C shale intervals are juxtaposed in this area, which suggests the occurrence of a topographic high in the northern part of the basin. Considering its location, we refer to this topographic feature as the Urapunga Arch. Although active between the deposition of the B and C shales, it probably existed before the deposition of the A shale and remained present until after the deposition of the C shale. The location of this structural high may be important for the accumulation of organic-rich strata in the Velkerri Formation. While recent work has emphasized the role of primary productivity over basin restriction (COX ET AL., 2019), this topographic high occurs over an area where it potentially separated the Beetaloo Sub-basin from the ocean between Laurentia and the NAC. Therefore, the Urapunga Arch may have restricted the water renewal of the basin, favouring the development of anoxic

environments. This structural feature would also prevent upwelling from providing nutrients, consequently driving the increased primary productivity in the A-C shales. This mechanism highlights the importance of rivers to deliver the nutrients sourced from the mafic rocks located to the south of the basin (YANG ET AL., 2019).

In the Velkerri, Moroak and Kyalla formations the 4th-order transgressive-regressive cycles (Figure 11 C) present a regular periodicity. This rhythmicity suggests that these were likely controlled by eustatic variation. The interpretation of medium-term eustatic variations in this Mesoproterozoic interval aligns with the results from MITCHELL ET AL. (2020) who highlighted short-term eustatic variations in the lower part of the studied interval.
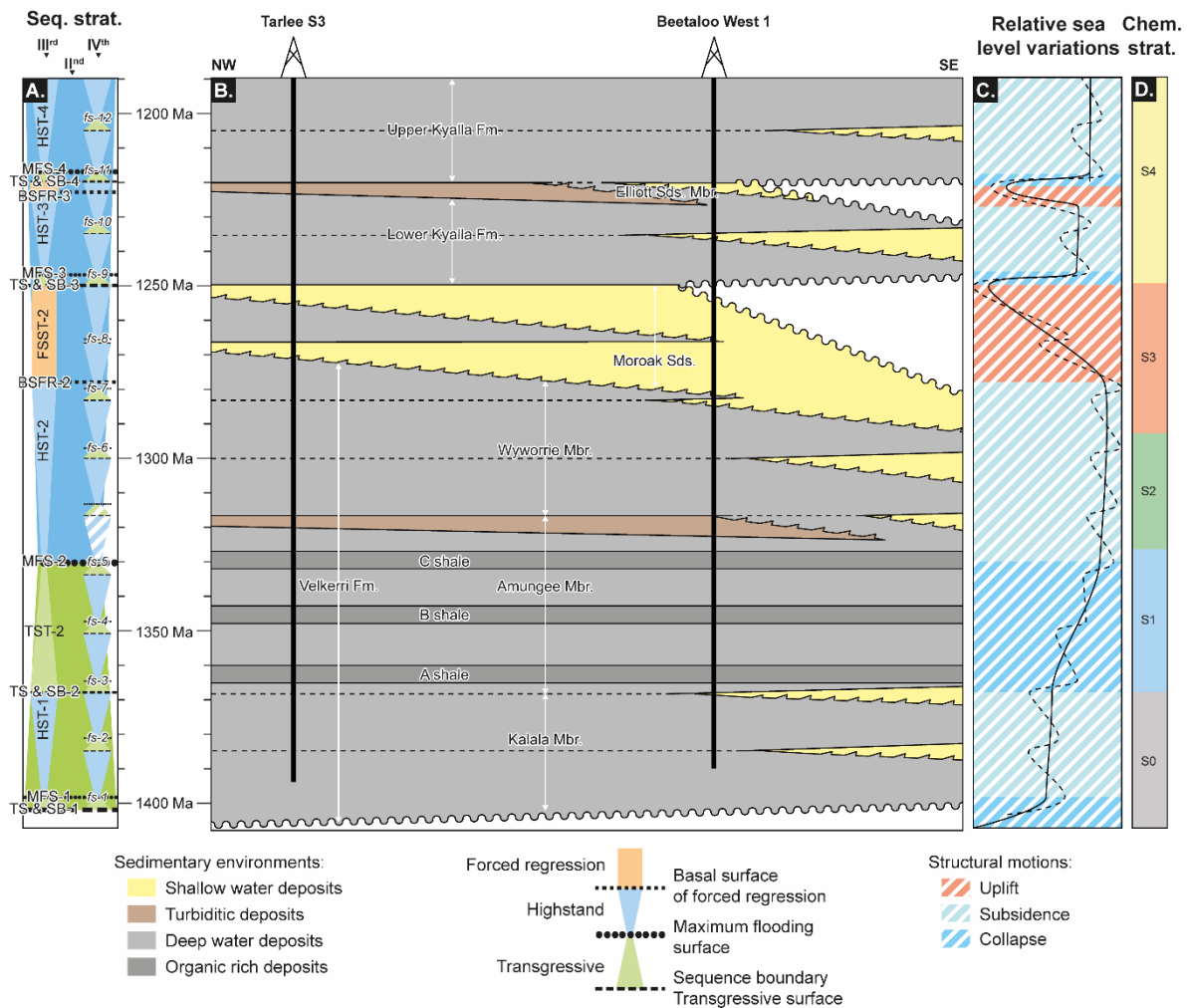
Figure 11: Wheeler diagram showing sequence stratigraphic architecture (A), the distribution of the sedimentary facies in the Velkerri, Moroak, and Kyalla formations (B), the variation of the relative sea level (C), and chemo-sequences (D) (chemo-sequences from MUNDAY AND FORBES, 2020).

Unlike the 4th-order cycles, the 3rd-order sequences have different periods (from 30 m.y. to 105 m.y.), which may suggest they were controlled by irregular, regional, structural processes. Within the Velkerri, Moroak and Kyalla formations, four intervals are interpreted as 3rd-order transgressions (Figure 11A) related to rapid relative sea-level rise events. They all show a sudden deepening of the sedimentary environment, with three of them recording a shift from subaerial unconformities to deep water deposits (ca. the bases of the Velkerri, the lower Kyalla, and upper Kyalla formations, Figure 11 B). We interpret the pace and amplitude of these changes to reflect rapid, structurally controlled

subsidence (Figure 11C). In addition to the 3rd-order transgressions, four regressive intervals are recorded within the studied interval (Figure 11 A). Here, the regressive parts of sequences 1 and 4 only record highstand deposition, while sequences 2 and 3 record both highstand deposition and forced regression. We interpret 3rd-order HSTs to have been deposited during phases of regional subsidence when sediment supply exceeded accommodation, and FSSTs to reflect large scale basin uplift (Figure 11 C).

When placed into a broader geodynamic context, the Velkerri, Moroak and Kyalla formations are interpreted to have been deposited during the closing of the Mirning Ocean and associated with subduction-related magmatism and orogeny located couple hundreds of kilometres to the south of the Beetaloo Sub-basin (YANG ET AL., 2019). The different basin-scale, uplift and subsidence phases observed in the Beetaloo Sub-basin can therefore be tied to the motions of the different cratons located around the basin. Indeed, craton accretions and variations in subduction speed will affect the stress regime and control the vertical motion of the area (ROHAIS ET AL., 2018). Two phases of uplift are recorded during the deposition of the Moroak sandstone (ca. 1250 Ma) and the Elliott sandstone member of the Kyalla Formation (ca. 1225 Ma), and precede the development of a major unconformity at the base of the Jamison sandstone (ca. 1150 Ma). The interpreted ages for each of these uplifts and resulting erosion events match the ages proposed by SMITS ET AL. (2014) for the accretion of the West, North and South Australian cratons. They showed cratons did not accrete prior to 1200 Ma, which suggests that the uplift event recorded by the sub-Jamison unconformity happened after the deposition of the Kyalla Formation and may record the cratons' accretions. This observation could also indicate that the uplift events present in the studied interval are related to the variation of the subduction velocity towards the S-SW edge of the North Australia Craton.

5.3.3. Paleogeographic evolution

The top of the Bessie Creek Sandstone is marked by a transgressive surface of erosion likely replacing a subaerial unconformity separating shallow water facies below the from deep water facies of unit 1 (ca. Kalala Member, Figure 12 A). We interpret most parts of the basin to have been mostly continental at the top of the Bessie Creek Sandstone (Figure 12A; this continental top has been eroded by the basal Velkerri transgression), transitioning into shallow marine and eventually offshore facies to the north of the study area. These deeper deposits are postulated to reflect the transition into an open ocean that lies further to the north (YANG ET AL., 2018). The strata overlying this surface are interpreted to record a transgression during the deposition of units 1 and 2 (ca. the Kalala and Amungee members, Figure 12B), in which the A, B, and C shales reflect intervals of maximum shoreline backstepping. At the end of the transgression, the shoreline is interpreted to have shifted significantly towards the south, close to the Tennant Creek and Arunta provinces.

Constraints determined from detrital zircons (YANG ET AL., 2019) and chemostratigraphy show that this transgression was not associated with a shift in provenance (Figure 11D). Following this transgression, a turbidite system with deposition towards the northwest was established, most likely confined by the Urapunga Arch to the north (Figure 12C). The next significant step in the evolution of the basin was the northwestward progradation of the shallow marine facies of the Moroak Sandstone (Figure 12D). The base of the turbiditic interval and the base of the Moroak Sandstone are marked by a change of chemo-sequence (Figure 11D) (MUNDAY AND FORBES, 2020). This change is not synchronous with the structural reorganisation observed in the extent of the basin. However, the sudden occurrence of gravity flow deposits suggests the reorganisation of continental drainage systems far outside of the study area; these are interpreted to be related to the closure of the Mirning ocean.
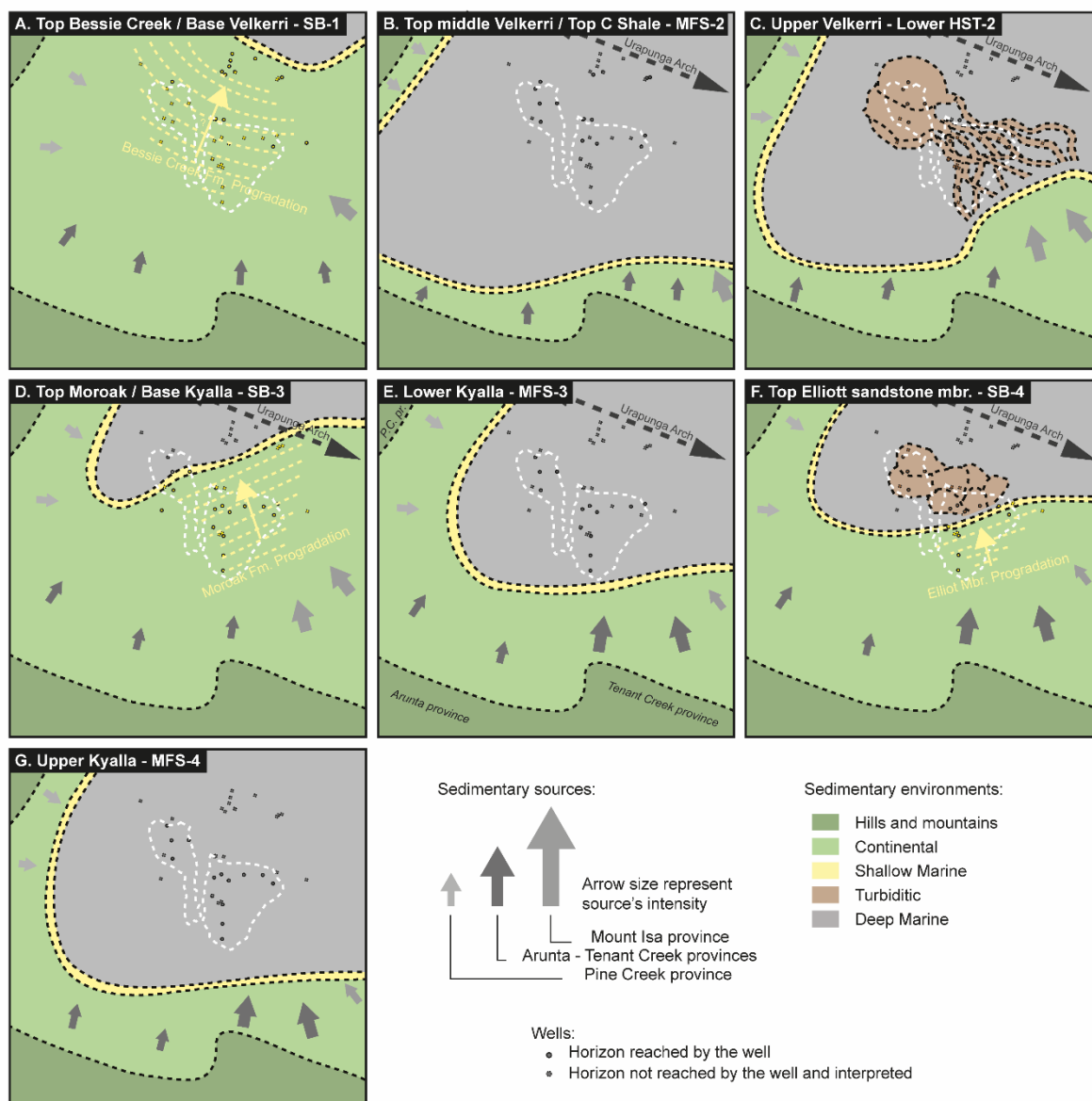
Figure 12: Schematic Paleogeographic evolution during the deposition of the Velkerri, Moroak and Kyalla formations.

The base of the Kyalla Formation is marked by another 2nd-order transgression (Figure 12E). However, we interpret this to have been associated with a less significant shoreline backstepping than the 2nd-order transgression that led to the deposition of the A, B and C shales of the Amungee Member. Indeed, core descriptions (Figure 4) show shallower facies in the lower Kyalla Formation, and chemostratigraphic analyses highlight similarities between S2 and S4, which can be interpreted as derived from the same sedimentary environments (Figure 11 D, MUNDAY AND FORBES, 2020). The organic content in the lower Kyalla Formation is moderately high, suggesting that the Urapunga Arch still existed during deposition of this interval. The Urapunga Arch would have provided ideal conditions for the development of a silled basin enabling organic matter to accumulate. Overlying the lower Kyalla Formation, the Elliot Member reflects regression, with shallow water deposits prograding from the SE towards the NW, progressively transitioning into gravity flow deposits (Figure 12F). The accumulation of turbidite deposits on the shelf suggests that the Urapunga Arch was still present, preventing gravity flows from transiting into open ocean settings. The overlying strata, up to the sub-Jamison unconformity, records a transgression with the second-largest backstep of the shoreline

observed in this study (Figure 12G). We postulate the shoreline to have shifted almost as far south as during the deposition of the C shale.

6. Conclusions

A detailed understanding of the stratigraphic architecture and facies heterogeneities in shale plays is important for reducing the risks and costs associated with exploration. Based on core descriptions, GR interpretations and well correlations this study reconstructed the stratigraphic evolution of the Mesoproterozoic Velkerri to Kyalla formation interval in the Beetaloo Sub-basin. This study integrated sequence stratigraphy with chemostratigraphy and chronostratigraphy to show that:

(1) The studied interval is mostly composed of sedimentary rocks that were deposited in wave-dominated, fluvial-influenced marine environments ranging from foreshore to offshore, including gravity flow deposits and delta front facies.

(2) Four main GR facies can be distinguished by upscaling core descriptions into GR log signatures. These include shallow water deposits, shoreface to offshore deposits, turbidite deposits and organic-rich deposits.

(3) The studied interval is composed of one 2nd-order depositional sequence, four 3rd-order depositional sequences, and 13 4th-order transgressive-regressive cycles.

(4) Stratigraphic sequences and chemo-sequences are linked in the Beetaloo Sub-basin. Both approaches are complementary and all chemo-sequence changes occur across surfaces of sequence stratigraphic significance.

(5) Sediments were likely supplied from the southeast during the deposition of the Velkerri, Moroak and Kyalla formations.

(6) Integrating previously published geochronology with our stratigraphic architecture suggests that the Velkerri Formation was likely deposited between 1400 Ma and 1280 Ma, the Moroak Sandstone between 1280 Ma and 1250 Ma and the Kyalla Formation between 1250 Ma and 1190 Ma.

(7) The Daly Waters High, presently the main structural feature in the Beetaloo Sub-basin, did not affect the sediment dispersal during the deposition of the Velkerri-Kyalla interval.

(8) Small structural highs likely existed in the Beetaloo sub-basin. For instance, a high that we have named the Urupunga Arch, existed in the northern part of the basin. It may have acted as a sill, limiting the water exchange between the basin and the open ocean.

(9) The studied stratigraphic interval records three phases of uplift. They are interpreted to be related to the continental geodynamic evolution of the area and reflect the progressive closure of the Mirning ocean located to the south of the Beetaloo Sub-basin.

This work can be used as a foundation for detailed studies focussing on the paleoenvironmental, mineralogical, petrophysical, and mechanical variations in the Beetaloo Sub-basin. Moreover, by identifying the controls on the basin's stratigraphic architecture, the findings of this study enable predictive models to be built. These models can be used to predict the distribution of sedimentary heterogeneities likely to generate hydrocarbons and provide favourable conditions for hydraulic stimulation.

References

Abbott, S. T., and I. P. Sweet, 2000, Tectonic control on third-order sequences in a siliciclastic ramp-style basin: An example from the Roper Superbasin (Mesoproterozoic), northern Australia: Australian Journal of Earth Sciences, v. 47, no. 3, p. 637–657, doi:10.1046/j.1440-0952.2000.00795.x.

Abbott, S. T., I. P. Sweet, K. A. Plumb, D. N. Young, A. Cutovinos, P. A. Ferenczi, A. Brakel, and B. A. Pietsch, 2001, Roper Region: Urapunga and Roper River Special, Northern Territory (Second Edition), Sheets SD 53-10, SD53-11, 1:250 000 Geological Map Series Explanatory Notes, Northern Territory Geological Survey, 100p: 0–100 p.

Ahamd, M., J. N. Dunster, T. J. Munson, and C. J. Edgoose, 2013, Overview of the geology and mineral and petroleum resources of the McArthur Basin, NT, in T. J. Munson, and K. J. Johnston, eds., AGES 2013: NT Geological Survey, p. 55–61.

Ainsworth, R. B., B. K. Vakarelov, and R. A. Nanson, 2011, Dynamic spatial and temporal prediction of changes in depositional processes on clastic shorelines: Toward improved subsurface uncertainty reduction and management: AAPG Bulletin, v. 95, no. 2, p. 267–297, doi:10.1306/06301010036.

Angulo, S., and L. A. Buatois, 2012, Integrating depositional models, ichnology,andsequence stratigraphy in reservoir characterization: The middle member of the Devonian-Carboniferous Bakken Formation of subsurface southeastern Saskatchewan revisited: AAPG Bulletin, v. 96, no. 6, p. 1017–1043, doi:10.1306/11021111045.

Bhattacharya, J., and R. G. Walker, 1992, Deltas, in R. G. Walker, and N. P. James, eds., Facies Models - Response to sea level change: p. 157–177.

Blaikie, T. N., and M. Kunzmann, 2020, Geophysical interpretation and tectonic synthesis of the Proterozoic southern McArthur Basin, northern Australia: Precambrian Research, v. 343, p. 105728, doi:https://doi.org/10.1016/j.precamres.2020.105728.

Bodorkos, S., J. L. Crowley, J. C. Claoué-Long, J. R. Anderson, and C. W. Magee, 2020, Precise U–Pb baddeleyite dating of the Derim Derim Dolerite, McArthur Basin, Northern Territory: old and new SHRIMP and ID-TIMS constraints: Australian Journal of Earth Sciences, p. 1–15, doi:10.1080/08120099.2020.1749929.

Borcovsky, D., S. Egenhoff, N. Fishman, J. Maletz, A. Boehlke, and H. Lowers, 2017, Sedimentology, facies architecture, and sequence stratigraphy of a Mississippian black mudstone succession-The upper member of the Bakken Formation, North Dakota, United States: p. 1625–1673, doi:10.1306/01111715183.

Bouma, A., 1964, Turbidites: Developments in Sedimentology, v. 3, p. 247–256, doi:10.1016/S0070-4571(08)70967-1.

Bruce, A., and D. Garrad, 2021, Unlocking the eastern extension of the Beetaloo Sub-basin middle Velkerri shales, in NTGS, ed., AGES 2021: p. 37–42.

Van Buchem, F. S. P., B. Pradier, and M. Stefani, 2005, Stratigraphic Patterns in Carbonate Source-Rock Distribution: Second-Order to Fourth-Order Control and Sediment Flux, in N. B. Harris, ed., The Deposition Of Organic-Carbon-Rich Sediments : Models, Mechanisms and Consequences: Special Publications of SEPM, p. 191–224.

Byun, U. H., H. S. Lee, and Y. K. Kwon, 2018, Sequence stratigraphy in the middle Ordovician shale successions, mid-east Korea: Stratigraphic variations and preservation potential of organic matter within a sequence stratigraphic framework: Journal of Asian Earth Sciences, v. 152, p. 116–131, doi:10.1016/j.jseaes.2017.11.028.

Catuneanu, O., 2019a, Model-independent sequence stratigraphy: Elsevier B.V., p. 312–388, doi:10.1016/j.earscirev.2018.09.017.

Catuneanu, O., 2006, Principles of sequence stratigraphy: Elsevier.

Catuneanu, O., 2019b, Scale in sequence stratigraphy: Elsevier Ltd, p. 128–159, doi:10.1016/j.marpetgeo.2019.04.026.

Catuneanu, O. et al., 2010, Sequence stratigraphy: common ground after three decades of development: First Break, v. 28, no. 1717, doi:10.3997/1365-2397.2010002.

Catuneanu, O. et al., 2009, Towards the standardization of sequence stratigraphy: Earth-Science Reviews, v. 92, no. 1–2, p. 1–33, doi:10.1016/j.earscirev.2008.10.003.

Catuneanu, O., W. E. Galloway, C. G. S. C. Kendall, A. D. Miall, H. W. Posamentier, A. Strasser, and M. E. Tucker, 2011, Sequence Stratigraphy: Methodology and Nomenclature: Newsletters on Stratigraphy, v. 44, no. 3, p. 173–245, doi:10.1127/0078-0421/2011/0011.

Chemostrat Australia, 2014, Release of Hess Corporations Elemental Data for 6 wells in the Beetaloo Basin. Available from: https://geoscience.nt.gov.au/gemis/ntgsjspui/handle/1/85022.

Chemostrat Australia, 2016, Release of Chemostrat Pty Ltd. Chemostratigraphy Data for 3 wells in the McArthur Basin. Available from: https://geoscience.nt.gov.au/gemis/ntgsjspui/handle/1/85067.

Close, D., 2014, The McArthur Basin: NTGS' approach to a frontier petroleum basin with known base metal prospectivity, in AGES 2014: NT Geological Survey, p. 85–89.

Close, D. I., A. J. Côté, E. T. Baruch, C. M. Altmann, F. M. Mohinudeen, B. Richards, and R. Ilett, 2017, Proterozoic shale gas plays in the Beetaloo Basin and the Amungee NW-1H discovery, in AGES 2017: NT Geological Survey, p. 7.

Copeland, P., 2020, On the use of geochronology of detrital grains in determining the time of deposition of clastic sedimentary strata: Basin Research, v. 32, no. 6, p. 1532–1546, doi:10.1111/bre.12441.

Cox, G. M., A. Jarrett, D. Edwards, P. W. Crockford, G. P. Halverson, A. S. Collins, A. Poirier, and Z. X. Li, 2016, Basin redox and primary productivity within the Mesoproterozoic Roper Seaway: Chemical Geology, v. 440, p. 101–114, doi:10.1016/j.chemgeo.2016.06.025.

Cox, G. M., P. Sansjofre, M. L. Blades, J. Farkas, and A. S. Collins, 2019, Dynamic interaction between basin redox and the biogeochemical nitrogen cycle in an unconventional Proterozoic petroleum system: Scientific Reports, v. 9, no. 1, doi:10.1038/s41598-019-40783-4.

Craig, J., U. Biffi, R. F. Galimberti, K. A. R. Ghori, J. D. Gorter, N. Hakhoo, D. P. Le Heron, J. Thurow, and M. Vecoli, 2013, The palaeobiology and geochemistry of Precambrian hydrocarbon source rocks: Elsevier, p. 1–47, doi:10.1016/j.marpetgeo.2012.09.011.

Crockford, P. W., J. A. Hayles, H. Bao, N. J. Planavsky, A. Bekker, P. W. Fralick, G. P. Halverson, T. H. Bui, Y. Peng, and B. A. Wing, 2018, Triple oxygen isotope evidence for limited mid-Proterozoic

primary productivity: Nature, v. 559, no. 7715, p. 613–616, doi:10.1038/s41586-018-0349-y.

Crombez, V., S. Rohais, F. Baudin, B. Chauveau, T. Euzen, and D. Granjeon, 2017, Controlling factors on source rock development: implications from 3D stratigraphic modeling of Triassic deposits in the Western Canada Sedimentary Basin: Bulletin de la Société géologique de France, v. 188, no. 5, p. 30, doi:10.1051/bsgf/2017188.

Crombez, V., S. Rohais, F. Baudin, and T. Euzen, 2016, Facies, well-log patterns, geometries and sequence stratigraphy of a wave-dominated margin: Insight from the Montney Formation (Alberta, British Columbia, Canada): Bulletin of Canadian Petroleum Geology, v. 64, no. 4, p. 516–537, doi:10.2113/gscpgbull.64.4.516.

Crombez, V., S. Rohais, F. Baudin, T. Euzen, J. P. Zonneveld, and M. Power, 2019, 3D stratigraphic architecture, sedimentary budget, and sources of the lower and middle triassic strata of Western Canada: Evidence for a major basin structural reorganization: Petroleum Geoscience, v. 26, no. 3, p. 462–479, doi:10.1144/petgeo2019-024.

Crombez, V., S. Rohais, T. Euzen, L. Riquier, F. Baudin, and E. Hernández Bilbao, 2020, Trace metal elements as paleoenvironmental proxies: Why should we account for sedimentation rates variations? Geology.

Cyr, A. J., D. E. Granger, V. Olivetti, and P. Molin, 2010, Quantifying rock uplift rates using channel steepness and cosmogenic nuclide-determined erosion rates: Examples from northern and southern Italy: Lithosphere, v. 2, no. 3, p. 188–198, doi:10.1130/L96.1.

Donnelly, T. H., and I. H. Crick, 1988, Depositional environment of the middle proterozoic velkerri formation in Northern Australia: Geochemical evidence: Precambrian Research, v. 42, no. 1–2, p. 165–172, doi:10.1016/0301-9268(88)90015-0.

Dumas, S., and R. W. C. Arnott, 2006, Origin of hummocky and swaley cross-stratification— The controlling influence of unidirectional current strength and aggradation rate: Geology, v. 34, no. 12, p. 1073–1076, doi:10.1130/G22930A.1.

Faiz, M., V. Crombez, C. Delle Piane, N. Lupton, M. Camilleri, and L. Langhi, 2021, Petroleum systems model for source-rock-reservoir evaluation in the Beetaloo Sub-basin, *in* Submitted to: AEGC 2021.

Fowler, A. C., and X. S. Yang, 1998, Fast and slow compaction in sedimentary basins: SIAM Journal on Applied Mathematics, doi:10.1137/S0036139996287370.

FROGTECH, 2018, SEEBASE® study and GIS for greater McArthur Basin: 174 p.

Gorter, J., and K. Grey, 2012, Velkerri Formation Depositional Model - Beetaloo Sub-basin, Northern Territory, Australia: Biostratigraphy and Organic Enrichment: Central Australian Basins Symposium III, p. 6.

Helland-Hansen, W., and J. G. Gjelberg, 1994, Conceptual basis and variability in sequence stratigraphy: a different perspective: Sedimentary Geology, v. 92, p. 31–52, doi:10.1016/0037-0738(94)90053-1.

Helland-Hansen, W., and G. J. Hampson, 2009, Trajectory analysis: concepts and applications: Basin Research, v. 21, no. 5, p. 454–483, doi:10.1111/j.1365-2117.2009.00425.x.

Helland-Hansen, W., and O. J. Martinsen, 1996, Shoreline trajectories and sequences; description of variable depositional-dip scenarios: Journal of Sedimentary Research, v. 66, no. 4, p. 670–688, doi:10.1306/D42683DD-2B26-11D7-8648000102C1865D.

Hodgskiss, M. S. W., P. Sansjofre, M. Kunzmann, E. A. Sperling, D. B. Cole, P. W. Crockford, T. M. Gibson, and G. P. Halverson, 2020, A high-TOC shale in a low productivity world: The late Mesoproterozoic Arctic Bay Formation, Nunavut: Earth and Planetary Science Letters, v. 544, doi:10.1016/j.epsl.2020.116384.

Hoffman, T. W., 2015, Recent drilling results provide new insights into the western Palaeoproterozoic to Mesoproterozoic McArthur Basin, *in* Ages 2015: NT Geological Survey.

Hunt, D., and M. E. Tucker, 1992, Stranded parasequences and the forced regressive wedge systems tract: deposition during base-level fall—reply: Sedimentary Geology, v. 95, p. 147–160, doi:10.1016/0037-0738(94)00123-C.

Jackson, M. J., M. D. Muir, and K. A. Plumb, 1987, Geology of the southern McArthur Basin, Northern Territory (Australia).: Bulletin - Bureau of Mineral Resources, Geology & Geophysics, Australia, v. 220.

Jackson, M. J., and R. Raiswell, 1991, Sedimentology and carbon-sulphur geochemistry of the Velkerri Formation, a mid-Proterozoic potential oil source in northern Australia: Precambrian Research, v. 54, no. 1, p. 81–108, doi:10.1016/0301-9268(91)90070-Q.

Jackson, M. J., P. N. Southgate, and R. W. Page, 2000, Gamma-ray logs and SHRIMP dates essential tools to constrain lithofacies interpretation of Proterozoic depositional systems, *in* N. James, and J. P. Grotzinger, eds., Proterozoic Carbonates: Society of Economic Paleontologists and Mineralogists Special Publication.

Jackson, J.-, I. P. Sweet, and T. G. Powell, 1988, Studies on Petroleum Geology and Geochemistry, Middle Proterozoic, McArthur Basin Northern Australia I: Petroleum Potential: The APPEA Journal, v. 28, no. 1, p. 283, doi:10.1071/aj87022.

Jarrett, A. J. M., S. MacFarlane, et al., 2019a, Source rock geochemistry and petroleum systems of the greater McArthur Basin and links to other northern Australian Proterozoic basins, *in* AGES 2019: NT Geological Survey, p. 14.

Jarrett, A. J. M., G. M. Cox, J. J. Brocks, E. Grosjean, C. J. Boreham, and D. S. Edwards, 2019b, Microbial assemblage and palaeoenvironmental reconstruction of the 1.38 Ga Velkerri Formation, McArthur Basin, northern Australia: Geobiology, v. 17, no. 4, p. 360–380, doi:10.1111/gbi.12331.

Jiongxin, X., 2005, Precipitation-vegetation coupling and its influence on erosion on the Loess Plateau, China: Catena, v. 64, no. 1, p. 103–116, doi:10.1016/j.catena.2005.07.004.

Johnson, J. G., and M. A. Murphy, 1984, Time-rock model for Siluro- Devonian continental shelf, western United States.: Geological Society of America Bulletin, v. 95, p. 1349–1359.

Kendall, B., R. A. Creaser, G. W. Gordon, and A. D. Anbar, 2009, Re-Os and Mo isotope systematics of black shales from the Middle Proterozoic Velkerri and Wollogorang Formations, McArthur Basin, northern Australia: Geochimica et Cosmochimica Acta, v. 73, no. 9, p. 2534–2558, doi:10.1016/j.gca.2009.02.013.

Kietzmann, D. A., R. M. Palma, A. C. Riccardi, J. Martín-Chivelet, and J. López-Gómez, 2014,

Sedimentology and sequence stratigraphy of a Tithonian-Valanginian carbonate ramp (Vaca Muerta Formation): A misunderstood exceptional source rock in the Southern Mendoza area of the Neuquén Basin, Argentina: Sedimentary Geology, v. 302, p. 64–86, doi:10.1016/j.sedgeo.2014.01.002.

Knapp, L. J., N. B. Harris, and J. M. McMillan, 2019, A sequence stratigraphic model for the organic-rich Upper Devonian Duvernay Formation, Alberta, Canada: Sedimentary Geology, v. 387, p. 152–181, doi:10.1016/j.sedgeo.2019.04.008.

Kohl, D., R. Slingerland, M. Arthur, R. Bracht, and T. Engelder, 2014, Sequence stratigraphy and depositional environments of the Shamokin (Union Springs) Member, Marcellus Formation, and associated strata in the middle Appalachian Basin: AAPG Bulletin, v. 98, p. 483–513, doi:10.1306/08231312124.

Kunzmann, M., V. Crombez, O. Catuneanu, T. N. Blaikie, G. Barth, and A. S. Collins, 2020, Sequence stratigraphy of the ca. 1730 Ma Wollogorang Formation, McArthur Basin, Australia: Marine and Petroleum Geology, v. 116, p. 104297, doi:10.1016/j.marpetgeo.2020.104297.

Lanigan, K., S. Hibbird, S. Menpes, and J. Torkington, 1994, Petroleum Exploration in The Proterozoic Beetaloo Sub-Basin, Northern Territory: The APPEA Journal, v. 34, no. 1, p. 674–691.

Lindsay, J. F., 2001, Basin dynamics and mineralisation, McArthur Basin, northern Australia: Australian Journal of Earth Sciences, v. 48, no. 5, p. 703–720, doi:10.1046/j.1440-0952.2001.00892.x.

Lyons, T. W., C. T. Reinhard, and N. J. Planavsky, 2014, The rise of oxygen in Earth's early ocean and atmosphere: doi:10.1038/nature13068.

Macquaker, J. H. S., S. J. Bentley, and K. M. Bohacs, 2010, Wave-enhanced sediment-gravity flows and mud dispersal across continental shelves: Reappraising sediment transport processes operating in ancient mudstone successions: Geology, v. 38, no. 10, p. 947–950.

Meert, J. G., and M. Santosh, 2017, The Columbia supercontinent revisited: p. 67–83, doi:10.1016/j.gr.2017.04.011.

Mitchell, R. N., U. Kirscher, M. Kunzmann, Y. Liu, and G. M. Cox, 2020, Gulf of Nuna: Astrochronologic correlation of a Mesoproterozoic oceanic euxinic event: Geology, v. 48, p. XXX–XXX, doi:10.1130/g47587.1.

Molnar, P., 2004, Late Cenozoic increase in accumulation rates of terrestrial sediment: How might climate change have affected erosion rates? Annual Review of Earth and Planetary Sciences, v. 32, no. 1, p. 67–89, doi:10.1146/annurev.earth.32.091003.143456.

Montgomery, D. R., and M. T. Brandon, 2002, Topographic controls on erosion rates in tectonically active mountain ranges: Earth and Planetary Science Letters, v. 201, no. 3–4, p. 481–489, doi:10.1016/S0012-821X(02)00725-2.

Mulder, J. A., J. A. Halpin, and N. R. Daczko, 2015, Mesoproterozoic Tasmania: Witness to the East Antarctica-Laurentia connection within Nuna: Geology, v. 43, no. 9, p. 759–762, doi:10.1130/G36850.1.

Munday, S., and A. Forbes, 2020, Chemostratigraphy in the Beetaloo Basin, *in* Sub20: CSIRO, p. 1.

Munday, S., 2020, Application of a Shale Evaluation Workflow in the Velkerri Fm, Beetaloo Basin. PESA

webinar.

Munson, T. J., 2016, Sedimentary characterisation of the Wilton package, greater McArthur Basin, Northern Territory: 157 p.

Munson, T. J., and D. Revie, 2018, Stratigraphic subdivision of the Velkerri Formation, Roper Group, McArthur Basin, Northern Territory: 31 p.

Myers, J. S., R. D. Shaw, and I. M. Tyler, 1996, Tectonic evolution of Proterozoic Australia: Tectonics, v. 15, no. 6, p. 1431–1446, doi:10.1029/96TC02356.

Origin Energy Resources Ltd, 2015a, Kalala S-1 Well Completion Report (Basic) EP 98 Beetaloo Basin Northern Territory. Available from: https://geoscience.nt.gov.au/gemis/ntgsjspui/ handle/1/86448

Origin Energy Resources Ltd, 2015b, AmungeeNW-1Well Completion Report(Basic)EP 98Beetaloo BasinNorthern Territory. Available from: https://geoscience.nt.gov.au/gemis/ntgsjspui/ handle/1/86845

Origin Energy Resources Ltd, 2016, Beetaloo W-1 Well Completion Report (Basic) EP 117 Beetaloo Basin Northern Territory. Available from: https://geoscience.nt.gov.au/gemis/ntgsjspui/ handle/1/87806

Ottmann, J., and K. Bohacs, 2014, Conventional Reservoirs Hold Keys to the 'Un's: AAPG Explorer.

Passey, Q. R., K. Bohacs, W. L. Esch, R. Klimentidis, and S. Sinha, 2010, From Oil-Prone Source Rock to Gas-Producing Shale Reservoir - Geologic and Petrophysical Characterization of Unconventional Shale Gas Reservoirs, *in* International Oil and Gas Conference and Exhibition in China: Society of Petroleum Engineers, doi:10.2118/131350-MS.

Pisarevsky, S. A., S. Å. Elming, L. J. Pesonen, and Z. X. Li, 2014, Mesoproterozoic paleogeography: Supercontinent and beyond: Precambrian Research, v. 244, no. 1, p. 207–225, doi:10.1016/j.precamres.2013.05.014.

Plumb, K., and P. Wellman, 1987, McArthur Basin, Northern Territory: mapping of deep troughs using gravity and magnetic anomalies: Bulletin - Bureau of Mineral Resources, Geology & Geophysics, Australia, v. 10, p. 243–251.

Plummer, P. S., and V. A. Gostin, 1981, Shrinkage cracks: desiccation or synaeresis? Journal of Sedimentary Petrology, v. 51, no. 4, p. 1147–1156, doi:10.1306/212f7e4b-2b24-11d7-8648000102c1865d.

Posamentier, H. W., and G. P. Allen, 1999, Siliciclastic Sequence Stratigraphy: Concepts and Applications: Society for Sedimentary Geology, 216 p.

Powell, T. G., M. J. Jackson, L. P. Sweet, I. H. Crick, C. J. Boreham, and R. E. Summons, 1987, Petroleum Geology And Geochemistry, Middle Proterozoic Mcarthur Basin: 290 p.

Rawlings, D. J., 1999, Stratigraphic resolution of a multiphase intracratonic basin system: The McArthur Basin, northern Australia: Australian Journal of Earth Sciences, v. 46, no. 5, p. 703–723, doi:10.1046/j.1440-0952.1999.00739.x.

Revie, D., 2017a, Unconventional petroleum resources of the Roper Group, McArthur Basin: 71 p.

Revie, D., 2017b, Volumetric resource assessment of the lower Kyalla and middle Velkerri formations of the McArthur Basin, *in* AGES 2017: NT Geological Survey, p. 5.

Rohais, S., V. Crombez, T. Euzen, and J. P. Zonneveld, 2018, Subsidence dynamics of the montney formation (Early triassic, western Canada sedimentary basin): Insights for its geodynamic setting and wider implications: Bulletin of Canadian Petroleum Geology, v. 66, no. 1, p. 128–160.

Schaller, M., F. Von Blanckenburg, N. Hovius, and P. W. Kubik, 2001, Large-scale erosion rates from in situ-produced cosmogenic nuclides in European river sediments: Earth and Planetary Science Letters, v. 188, no. 3–4, p. 441–458, doi:10.1016/S0012-821X(01)00320-X.

Sheridan, M., D. R. Johns, H. D. Johnson, and S. Menpes, 2018, The stratigraphic architecture, distribution and hydrocarbon potential of the organic-rich Kyalla and Velkerri shales of the Upper Roper Group (McArthur Basin): The APPEA Journal, p. 4, doi:10.1071/aj17224.

Smith, M. G., and R. M. Bustin, 2000, Late Devonian and Early Mississippian Bakken and Exshaw black shale source rocks, Western Canada sedimentary basin: A sequence stratigraphic interpretation: AAPG Bulletin, v. 84, no. 7, p. 940–960, doi:10.1306/a9673b76-1738-11d7-8645000102c1865d.

Smits, R. G., W. J. Collins, M. Hand, R. Dutch, and J. Payne, 2014, A Proterozoic Wilson cycle identified by Hf isotopes in central Australia: Implications for the assembly of Proterozoic Australia and Rodinia: Geology, v. 42, no. 3, p. 231–234, doi:10.1130/G35112.1.

Spinks, S. C., S. Schmid, A. Pagés, and J. Bluett, 2016, Evidence for SEDEX-style mineralization in the 1.7Ga Tawallah Group, McArthur Basin, Australia: Ore Geology Reviews, v. 76, p. 122–139, doi:https://doi.org/10.1016/j.oregeorev.2016.01.007.

Stow, D. A. V., A.-Y. Huc, and P. Bertrand, 2001, Depositional processes of black shales in deep water: Marine and Petroleum Geology, v. 18, no. 4, p. 491–498, doi:10.1016/S0264-8172(01)00012-5.

Stow, D. A. V, and D. J. W. Piper, 1984, Deep-water fine-grained sediments: facies models, *in* D. A. . Stow, and D. J. W. Piper, eds., Fine-grained Sediments: Deep-water Processes and Facies: Geological Society Special Publication N°15, p. 611–646, doi:10.1144/GSL.SP.1984.015.01.38.

Summerfield, M. A., and N. J. Hulton, 1994, Natural controls of fluvial denudation rates in major world drainage basins: Journal of Geophysical Research: Solid Earth, v. 99, no. B7, p. 13871–13883, doi:10.1029/94jb00715.

Suter, E. H., 2006, Facies Models Revisited: Clastic Shelves, *in* H. W. Posamentier, and R. G. Walker, eds., Facies Models Revisited: SEPM Special Publication N°84, p. 339–398.

Tucker, D. H., and D. M. Boyd, 1987, Dykes of Australia detected by airborne magnetic surveys, *in* Mafic Dyke Swarms: Geological Association of Canada, p. 163–172.

Tyson, R. V., 2001, Sedimentation rate, dilution, preservation and total organic carbon: some results of a modelling study: Organic Geochemistry, v. 32, no. 2, p. 333–339, doi:10.1016/S0146-6380(00)00161-3.

de Vries, S. T., L. L. Pryer, and N. Fry, 2008, Evolution of Neoarchaean and Proterozoic basins of Australia: Precambrian Research, v. 166, no. 1–4, p. 39–53, doi:10.1016/j.precamres.2008.01.005.

Walker, R. G., 1992, Turbidites and submarine fans, *in* R. G. Walker, and N. P. James, eds., Facies

Models - Response to sea level change: Geological Association of Canada, p. 239–264.

Walker, R. G., and A. G. Plint, 1992, Wave- and storm-dominated shallow marine systems, *in* R. G. Walker, and N. P. James, eds., Facies Models - Response to sea level change: Geological Association of Canada, p. 219–238.

Warren, J. K., S. C. George, P. J. Hamilton, and P. Tingate, 1998, Proterozoic source rocks: sedimentology and organic characteristics of the Velkerri Formation, Northern Territory, Australia: AAPG Bulletin, v. 82, no. 3, p. 442–463.

Williams, B., 2020, Definition of the Beetaloo Sub-basin, in G. C. MacDonald, ed., AGES 2020: NT Geological Survey, p. 100–103.

Wilson, A., L. Thrane, A. Cote, B. Richards, and C. Altmann, 2021, Borehole image features map depositional environment change in a Mesoproterozoic delta: insights from the Beetaloo Sub-Basin, *in* First EAGE Workshop on Borehole Geology in Asia Pacific: EAGE, p. 1p.

Yang, B., A. S. Collins, M. L. Blades, N. Capogreco, J. L. Payne, T. J. Munson, G. M. Cox, and S. Glorie, 2019, Middle–late mesoproterozoic tectonic geography of the North Australia craton: U–pb and hf isotopes of detrital zircon grains in the beetaloo sub-basin, northern territory, Australia: Journal of the Geological Society, v. 176, no. 4, p. 771–784, doi:10.1144/jgs2018-159.

Yang, B., A. S. Collins, M. L. Blades, T. J. Munson, J. L. Payne, S. Glorie, and J. Farkaš, 2020b, Tectonic controls on sedimentary provenance and basin geography of the Mesoproterozoic Wilton package, McArthur Basin, northern Australia: Geological Magazine, p. 1–20, doi:10.1017/S0016756820001223.

Yang, B., A. S. Collins, G. M. Cox, A. J. M. Jarrett, S. Denyszyn, M. L. Blades, J. Farkaš, and S. Glorie, 2020a, Using Mesoproterozoic sedimentary geochemistry to reconstruct basin tectonic geography and link organic carbon productivity to nutrient flux from a Northern Australian large igneous Province: Basin Research, doi:10.1111/bre.12450.

Yang, B., T. M. Smith, A. S. Collins, T. J. Munson, B. Schoemaker, D. Nicholls, G. Cox, J. Farkas, and S. Glorie, 2018, Spatial and temporal variation in detrital zircon age provenance of the hydrocarbon-bearing upper Roper Group, Beetaloo Sub-basin, Northern Territory, Australia: Precambrian Research, v. 304, p. 140–155, doi:10.1016/j.precamres.2017.10.025.

Zeller, M., S. B. Reid, G. P. Eberli, R. J. Weger, and J. L. Massaferro, 2015, Sequence architecture and heterogeneities of a field - Scale Vaca Muerta analog (Neuquén Basin, Argentina) - From outcrop to synthetic seismic: Marine and Petroleum Geology, v. 66, p. 829–847, doi:10.1016/j.marpetgeo.2015.07.021.

Supplementary material

Supplementary Table 1: Wells used for this study.

Well Name	Kyalla Fm.	Moroak Fm.	Velkerri Fm.
Alexander 1			X
Altree 2			X
Amungee NW 1	X	X	X
Balmain 1	X		
Beetaloo W1	X	X	X
Birdum Creek 1	X	X	X
Borrowdale 2			X
Broadmere 1			X
Burdo 1	X	X	
Chanin 1	X	X	
Elliott 1	X	X	X
Friendship 1			X
Golden Grove 1			X
Jamison 1	X	X	
Kalala South 1	X	X	X
Lady Penrhyn 1			X
Lawrence 1			X
Marmbulligan 1			X
Mason 1	X		
McManus 1	X	X	X
Prince of Wales 1			X
Ronald 1	X	X	
Scarborough 1			X
Sever 1			X
Shenandoah 1	X	X	X
Shortland 1	X		
Tanumbirini 1	X	X	X
Tarlee 1	X	X	X
Tarlee 2	X	X	X
Tarlee S3	X	X	X
Walton 2			X
Wyworrie 1	X	X	X
Total	19	16	25

Supplementary Table 2: Cored intervals described for this study.

Well Name	Top (m)	Bottom (m)	Thickness (m)	Formation
Alexander 1	400	640	240	Velkerri
Elliott 1	1080	1400	320	Moroak & Kyalla
Jamison 1	1360	1560	200	Kyalla
Lady Penrhyn 2	290	450	160	Velkerri
McManus 1	650	850	200	Velkerri & Moroak
Shenandoah 1	1580	1600	20	Kyalla
Shenandoah 1	2500	2520	20	Velkerri
Tarlee S3	1100	1640	540	Velkerri
Walton 2	250	980	730	Velkerri
		Total	**2430**	

Supplementary Table 3: Zircon ages from samples located in the studied interval (data from YANG ET AL., 2018, 2019*).*

Well	Depth	Stratigraphic unit	Sample	Minimum Zircon Age (Ma)
Walton 2	227	Upper Jamison	W-UJ9	1040 ± 100
Walton 2	1013	Bessie Creek	W-BC1	1579 ± 27
Sever 1	1167	Bessie Creek	S-BC1	1354 ± 14
McManus 1	550	Lower Jamison	M-LJ3	1193 ± 79
McManus 1	671	Moroak	M-Mo8	1569 ± 57
McManus 1	724	Moroak	M-Mo11	1527 ± 45
Jamison 1	904	Upper Jamison	J-UJ3	1084 ± 83
Jamison 1	1490	Kyalla	J-Ky8	1324 ± 59
Jamison 1	1587	Kyalla	JN-Ky6	1420 ± 49
Jamison 1	1721	Moroak	J-Mo13	1404 ± 28
Elliott 1	644	Lower Jamison	E-LJ2	1142 ± 47
Elliott 1	887	Kyalla	E-Ky7	1313 ± 47
Elliott 1	1021	Kyalla	EN-Ky4	1517 ± 58
Elliott 1	1367	Moroak	EN-Mo8	1502 ± 75
Elliott 1	1518	Moroak	E-Mo13	1550 ± 57
Elliott 1	1697	Velkerri	E-Vel18	1298 ± 47
Birdum Creek 1	887	Kyalla	BirC-Ky1	1400 ± 43
Altree 2	335	Upper Jamison	A-UJ1	1092 ± 55
Altree 2	349	Upper Jamison	A-UJ2	987 ± 68
Altree 2	1468	Bessie Creek	A-BC13	1409 ± 42